From dense to dilute two-phase flows

Ashwin Chinnayya, Richard Saurel, Quentin Carmouze

From dense to dilute two-phase flows

Ashwin Chinnayya[(1)], Richard Saurel[(2)] and Quentin Carmouze [(3)]

[(1)] Institut Pprime, Laboratoire LCD, CNRS Fédération 2862, 43 rue de l'Aérodrome, 86036 Poitiers Cedex, France
[(2)]M2P2 and IUF, UMR CNRS 7340, Centrale Marseille, 38 rue Joliot Curie, 13450 Marseille Cedex 13, France
[(3)]RS2N, 371 chemin de Gaumin, 83640 Saint-Zacharie, France

Abstract

Many two-phase flow situations, from engineering science to astrophysics, deal with transition from dense (high concentration of the condensed phase) to dilute concentration (low concentration of the same phase), covering the entire range of volume fractions. Some models are now well accepted at the two bounds, but none is able to cover accurately the entire range, in particular regarding waves propagation. In the present work an alternative to the Baer and Nunziato (1986) (BN for short) model is built. The corresponding model is hyperbolic and thermodynamically consistent. Contrarily to the BN model that involves 6 wave speeds, the new formulation involves 4 waves only, in agreement with the Marble (1963) model based on pressureless Euler equations for the dispersed phase, this model being well accepted for low particle volume concentrations. In the new model, the presence of pressure in the momentum equation of the particles and consideration of volume fractions in the two phases render the model valid for large particle concentrations. A symmetric version of the new model is derived as well for liquids containing gas bubbles. This model version involves 4 wave speeds as well, but with different wave's speeds. Last, the two sub models with 4 waves are combined in a unique formulation, valid for all volume fractions. It involves the same 6 wave's speeds as the BN model, but at a given point of space 4 waves only emerge, depending on the local volume fractions. Basically, when the gas phase is in dominant concentration, it carries sound waves and reversely for the liquid phase.

The new model is tested numerically on various test problems ranging from separated phases in a shock tube to shock – particle cloud interaction. Its predictions are compared to BN and Marble models.

Key words: hyperbolic, two-phase, compressible, shocks

Emails: Ashwin.Chinnayya@ensma.fr; Richard.Saurel@univ-amu.fr; quentin.carmouze@rs2n.eu

I. Introduction

It is well accepted that hyperbolic models are mandatory to deal with phenomena involving wave propagation. This is the case for multiphase flow mixtures in many situations such as in particular shocks and detonations propagation in granular explosives and in fuel suspensions, as well as liquid-gas mixtures with bubbles, cavitation and flashing, as soon as motion is intense and governed by pressure gradients. This is thus the case of most unsteady two-phase flows situations.

Wave propagation is important as it carries pressure, density and velocity disturbances. Sound propagation is also very important as it determines critical (choked) flow conditions and associated mass flow rates. It has also fundamental importance on sonic conditions of detonation waves when the two-phase mixture is exothermically reacting (Petitpas et al., 2009).

Hyperbolicity is also related to the causality principle, meaning that initial and boundary conditions are responsible of time evolution of the solution. When dealing with first-order partial differential equations it means that the Riemann problem must have a solution, and the Riemann problem is correctly posed only if the equations are hyperbolic.

However, only a few two-phase flow models are hyperbolic in the whole range of parameters. The Baer and Nunziato (1986) model seems to be the only formulation able to deal with such requirement. Its symmetric extension (Saurel et al., 2014) facilitates the Riemann problem resolution as the corresponding model involves 7 wave's speeds (instead of 6 in the original version) (see also Ambroso et al., 2012 for similar conclusions).

However, in the dilute limit at least, the acoustic properties of this model seem inconsistent (Lhuillier et al., 2013). Indeed with this model, the dispersed phase sound speed corresponds to the one of the pure phase, while this phase is not continuous and unable to propagate sound in reality. When the phase is not continuous (dispersed drops in a gas, dispersed bubbles in a liquid), the associated sound speed should be lowered (and possibly vanish), such effect being absent of the formulation.

In the low particles concentration limit, the Marble (1963) model is preferred. This model corresponds to the Euler equations with source terms for the gas phase and pressureless gas dynamic equations for the particle phase (see also Zeldovich, 1970). This model is thermodynamically consistent and hyperbolic as well, except that the particle phase equations are hyperbolic degenerate. In this model, contrarily to the BN model, the sound speed is absent of the particles phase equations and this behaviour seems more physical in this limit. However, the Marble model has a limited range of validity as the volume of the dispersed phase is neglected, this assumption having sense only for low (less than per cent) condensed phase volume fraction.

There are thus fundamental differences between these two models:

- The volume occupied by the condensed phase is considered in BN while it is neglected in the dilute model, restricting its validity to low volume fraction of the dispersed phase.
- Condense phase compressibility if considered in BN while incompressible particles are assumed in the dilute formulation.
- Acoustic properties of the BN model are well accepted in the dense domain but seem inappropriate in the dilute limit.

Even if these two models can be used in the entire space of two-phase flow variables without yielding computational failure (this is characteristic of thermodynamically consistent hyperbolic models) validity of their results is questionable when they are used out of their range of physical validity. This issue has been clearly understood in Lhuillier et al. (2013), McGrath et al. (2016) and Houim and Oran (2016) where various attempts to build new formulations are reported. However none seem able to cover the entire range of volume fractions while remaining hyperbolic, thermodynamically consistent and having physically acceptable acoustic properties. The aim of the present paper is to build an alternative to the BN model with improved acoustic properties.

The new model is derived from number density and particle radius (or bubble radius) evolution equations resulting in a volume fraction evolution equation expressed in conservation form with relaxation. The switch from a transport equation in the BN model to a conservation equation in the present formulation has dramatic influence on wave's propagation and structure of the equations.
The paper is organised as follows. The well-known BN and Marble models are recalled in Section II to present the main alternatives of existing two-phase hyperbolic models. Derivation of the volume fraction of the new model is adressed in Section III. The new model is then derived in Section IV and its hyperbolicity demonstrated. Its compatibility with the model of Kapila et al. (2001) is demonstrated as asymptotic limit of the new model, in the limit of stiff mechanical relaxation. To examine typical solutions an appropriate hyperbolic solver is needed and its derivation is addressed in Section V. Computed results are then examined in Section VI, compared to exact and experimental solutions when available. A symmetric variant of the new flow model, aimed to model bubbly liquids, is derived in Section VII and typical solutions are examined. A general model, aimed to address any flow volume fractions is then derived in Section VIII. Conclusions are given in Section IX.

II. Well-known limit models

Two hyperbolic models are widely used in the two-phase flow literature (another option being given in Romenski and Toro, 2004). Their main characteristics are recalled hereafter.

a) BN type model

The Baer and Nunziato (1986) is recalled hereafter, in the absence of granular effects ('configuration' pressure and energy) as well as heat and mass transfers. Mechanical relaxation effects only are considered in addition to wave's dynamics. The symmetric variant of Saurel et al. (2003) is presented rather than the original BN.

Phase 1

$$\begin{aligned}
&\frac{\partial \alpha_1}{\partial t} + u_I \frac{\partial \alpha_1}{\partial x} = \mu(p_1 - p_2) \\
&\frac{\partial (\alpha\rho)_1}{\partial t} + \frac{\partial (\alpha\rho u)_1}{\partial x} = 0 \\
&\frac{\partial (\alpha\rho u)_1}{\partial t} + \frac{\partial (\alpha\rho u^2 + \alpha p)_1}{\partial x} = p_I \frac{\partial \alpha_1}{\partial x} + \lambda(u_2 - u_1) \\
&\frac{\partial (\alpha\rho E)_1}{\partial t} + \frac{\partial (\alpha(\rho E + p)u)_1}{\partial x} = p_I u_I \frac{\partial \alpha_1}{\partial x} + \lambda u_I'(u_2 - u_1) - \mu p_I'(p_1 - p_2)
\end{aligned} \qquad \text{(II.1)}$$

Phase 2

$$\begin{aligned}
&\frac{\partial (\alpha\rho)_2}{\partial t} + \frac{\partial (\alpha\rho u)_2}{\partial x} = 0 \\
&\frac{\partial (\alpha\rho u)_2}{\partial t} + \frac{\partial (\alpha\rho u^2 + \alpha p)_2}{\partial x} = p_I \frac{\partial \alpha_2}{\partial x} - \lambda(u_2 - u_1) \\
&\frac{\partial (\alpha\rho E)_2}{\partial t} + \frac{\partial (\alpha(\rho E + p)u)_2}{\partial x} = p_I u_I \frac{\partial \alpha_2}{\partial x} - \lambda u_I'(u_2 - u_1) + \mu p_I'(p_1 - p_2)
\end{aligned} \qquad \text{(II.2)}$$

With the following definitions and notations:

- α_k, ρ_k, u_k, E_k, p_k denote respectively the volume fraction, material density, velocity, total energy and pressure of the phase k (k=1,2).

- The total energy of the phases read, $E_k = e_k + \frac{1}{2}u_k^2$.

- The pressures are given by convex equations of state of the form $p_k = p_k(\rho_k, e_k)$.

- The velocities relax each other to a common equilibrium one at a rate controlled by λ, modelled by conventional drag force correlations and specific interfacial area.
- The pressure relax each other to a common equilibrium one at a rate controlled by μ. Estimates for this relaxation parameter are given in the references above: $\mu = \frac{A_I}{Z_1 + Z_2}$, where A_I represents the interfacial exchange area.
- The interfacial variables are estimated by:

$$u_I = \frac{Z_1 u_1 + Z_2 u_2}{Z_1 + Z_2} + \mathrm{sgn}\left(\frac{\partial \alpha_1}{\partial x}\right) \frac{p_2 - p_1}{Z_1 + Z_2},$$

$$u_I' = \frac{Z_1 u_1 + Z_2 u_2}{Z_1 + Z_2},$$

$$\pi_I = \frac{Z_2 p_1 + Z_1 p_2}{Z_1 + Z_2} + \mathrm{sgn}\left(\frac{\partial \alpha_1}{\partial x}\right) \frac{Z_1 Z_2}{Z_1 + Z_2}(u_2 - u_1),$$

$$\pi_I' = \frac{Z_2 p_1 + Z_1 p_2}{Z_1 + Z_2}.$$

This symmetric formulation of the BN model has some advantages:

-Its extension to more than two materials is quite easy.

-It is able to deal with contact and permeable interfaces (Saurel et al., 2003, Saurel et al., 2014).

-It involves an extra wave, not aligned with the condensed phase velocity, this property having benefits at least for numerical resolution (Ambroso et al., 2012, Furfaro and Saurel, 2015).

This system admits the following mixture entropy equation:

$$\frac{\partial (\alpha\rho)_1 s_1 + (\alpha\rho)_2 s_2}{\partial t} + \frac{\partial (\alpha\rho)_1 u_1 s_1 + (\alpha\rho)_2 u_2 s_2}{\partial x} =$$

$$\frac{1}{T_1}\left\{\frac{Z_1}{(Z_1 + Z_2)^2}\left((p_2 - p_1) + \mathrm{sgn}\left(\frac{\partial \alpha_1}{\partial x}\right) Z_2 (u_2 - u_1)\right)^2 \left|\frac{\partial \alpha_1}{\partial x}\right| + \lambda \frac{Z_2}{Z_1 + Z_2}(u_2 - u_1)^2 + \mu \frac{Z_1}{Z_1 + Z_2}(p_2 - p_1)^2\right\}$$

$$+ \frac{1}{T_2}\left\{\frac{Z_2}{(Z_1 + Z_2)^2}\left((p_2 - p_1) + \mathrm{sgn}\left(\frac{\partial \alpha_1}{\partial x}\right) Z_2 (u_2 - u_1)\right)^2 \left|\frac{\partial \alpha_2}{\partial x}\right| + \lambda \frac{Z_1}{Z_1 + Z_2}(u_2 - u_1)^2 + \mu \frac{Z_2}{Z_1 + Z_2}(p_2 - p_1)^2\right\}$$

Its 7 associated wave speeds are:

$\lambda_I = u_I$, $\lambda_1 = u_1$, $\lambda_2 = u_1 + c_1$, $\lambda_3 = u_1 - c_1$, $\lambda_4 = u_2$, $\lambda_5 = u_2 + c_2$, $\lambda_6 = u_2 - c_2$.

This model is consequently hyperbolic, thermodynamically consistent and symmetric. However, the wave speeds are independent of the volume fraction, meaning that in the dilute limit, the sound speed in the condensed phase is unchanged, this behaviour being questionable.

b) Dilute two-phase flow model (Marble, 1963)

As the model that follows is no longer symmetric it is necessary to precise the phases. Phase 1 is considered to be the condensed one and the gas phase is denoted by the subscript 2. The 'apparent density' of the dispersed phase is introduced as, $\bar{\rho}_1 = (\alpha\rho)_1$.

In this approach, $\alpha_1 < 0.01$ and volume fraction effects are neglected in the gas phase equations.

Phase 1 (dispersed)

$$\frac{\partial \bar{\rho}_1}{\partial t} + \frac{\partial \bar{\rho}_1 u_1}{\partial x} = 0$$

$$\frac{\partial \bar{\rho}_1 u_1}{\partial t} + \frac{\partial \bar{\rho}_1 u_1^2}{\partial x} = \lambda (u_2 - u_1) \qquad \text{(II.3)}$$

$$\frac{\partial \bar{\rho}_1 e_1}{\partial t} + \frac{\partial \bar{\rho}_1 e_1 u_1}{\partial x} = 0 \text{ or alternatively } \frac{\partial \bar{\rho}_1 E_1}{\partial t} + \frac{\partial \bar{\rho}_1 E_1 u_1}{\partial x} = \lambda u_1 (u_2 - u_1).$$

Phase 2 (gas)

$$\frac{\partial \rho_2}{\partial t} + \frac{\partial \rho_2 u_2}{\partial x} = 0 \qquad \text{(II.4)}$$

$$\frac{\partial \rho_2 u_2}{\partial t} + \frac{\partial \rho_2 u_2^{\,2} + p_2}{\partial x} = -\lambda (u_2 - u_1)$$

$$\frac{\partial \rho_2 E_2}{\partial t} + \frac{\partial (\rho_2 E_2 + p_2) u_2}{\partial x} = -\lambda u_1 (u_2 - u_1)$$

This system admits the following mixture entropy equation:

$$\frac{\partial \bar{\rho}_1 s_1 + \rho_2 s_2}{\partial t} + \frac{\partial \bar{\rho}_1 s_1 u_1 + \rho_2 s_2 u_2}{\partial x} = \frac{\lambda (u_1 - u_2)^2}{T_2}$$

Its associated wave speeds are:

$\lambda_1 = u_1$, $\lambda_2 = u_2$, $\lambda_3 = u_2 + c_2$, $\lambda_4 = u_2 - c_2$.

As $\lambda_1 = u_1$ is fold three times, the system for phase 1 is hyperbolic degenerate, while the one of the gas phase is strictly hyperbolic.

These two models are thus well posed in the sense that they are thermodynamically consistent, frame invariant and hyperbolic. Both models can be solved by Godunov type methods as the Riemann problem has been addressed for both (Saurel et al., 1994, Saurel and Abgrall, 1999, Schwendeman et al., 2006, Deledicque and Papalexandris, 2010, Furfaro and Saurel, 2015). However, well posedness is a necessary condition but not a sufficient one for physical validity. In particular it is difficult to believe that sound propagates in the solid phase at speed c_1 when the two-phase mixture becomes dilute, i.e., when the particles have no contact. See also Lhuillier et al. (2013) and McGrath et al. (2016) for extra arguments.

III. Volume fraction equation

Let us first examine the physical meaning of the volume fraction equation in the BN model, the new formulation will be considered secondly.

The volume fraction equation of the BN model is associated to a specific representation of the two-phase mixture that can be schematized as done in the Figure 1.

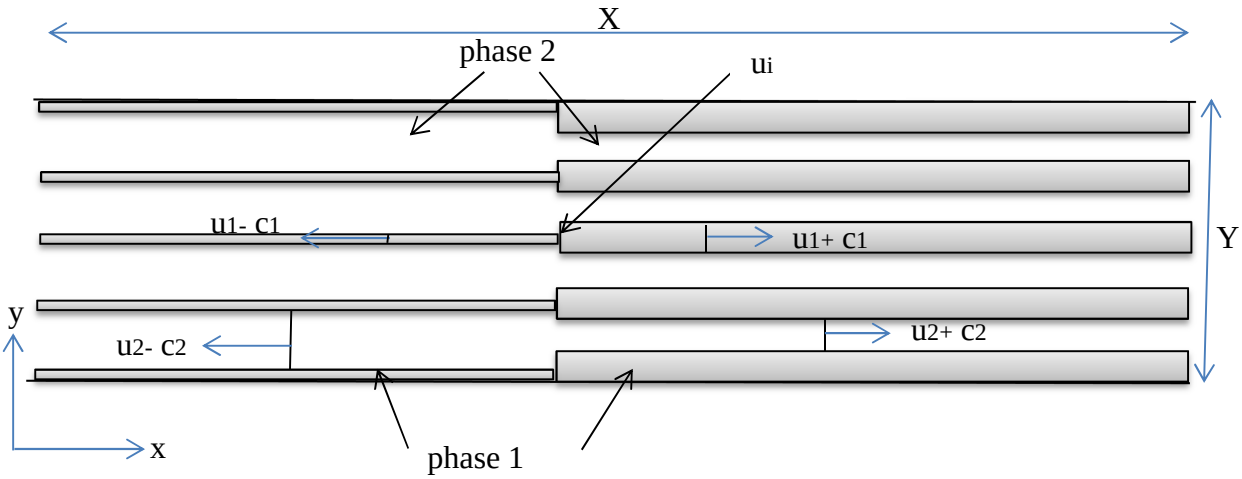

Figure 1. Schematic representation of a two-phase mixture in a duct of constant cross section with the BN model. The acoustic waves propagate freely in each pure fluid as if it was continuous. In order that each phase be able to support these acoustic waves the topology must

be free of vertical interfaces, otherwise wave diffraction occurs. Horizontal interfaces result in pressure relaxation terms.

The volume fraction equation in the BN model results of space averaging of the following characteristic function evolution equation:

$$\frac{\partial X_k}{\partial t} + \vec{u}_I.\mathrm{grad}(X_k) = 0, \qquad \text{(III.1)}$$

where $\vec{u}_I$ is the local interface velocity and X_k is the phase k characteristic function defined by,

$$X_k = \begin{cases} 1 \text{ if the point belongs to phase k} \\ 0 \text{ otherwise} \end{cases}.$$

The volume average of that equation reads,

$$\frac{1}{V}\frac{\partial}{\partial t}\int_V X_k dV + \frac{1}{V}\int_V \vec{u}_I.\mathrm{grad}(X_k)dV = 0. \qquad \text{(III.2)}$$

The gradient of the characteristic function is non-zero only at interfaces separating phases 1 and 2. The representation shown in Figure 1 contains vertical interfaces, separating fluid 2 at left and fluid 1 at right and horizontal interfaces separating fluid 1 at left (in the direction of the y axis) and fluid 2 at right, then fluid 2 at left and fluid 1 at right and so on.

The local interface velocity is computed by the acoustic Riemann solver given by:

$$u_I = \frac{Z_L u_L + Z_R u_R}{Z_L + Z_R} + \frac{p_L - p_R}{Z_L + Z_R}$$

Inserting this formula in (III.2) leads to,

$$\frac{1}{V}\frac{\partial V_k}{\partial t} + \frac{1}{V}\left\{ \begin{array}{l} \left(\frac{Z_1 u_1 + Z_2 u_2}{Z_2 + Z_1} + \frac{p_2 - p_1}{Z_1 + Z_2}\right) \sum_{\text{vertical segments}} \int_{y_{\text{begin segment}}}^{y_{\text{end segment}}} (X_{kR} - X_{kL})dy \\ + N_{\text{number of fluid channels}} \left[\begin{array}{l} \left(\frac{Z_1 v_1 + Z_2 v_2}{Z_1 + Z_2} + \frac{p_1 - p_2}{Z_1 + Z_2}\right)\int_0^X (X_{kR} - X_{kL})dx \\ + \left(\frac{Z_1 v_1 + Z_2 v_2}{Z_1 + Z_2} - \frac{p_1 - p_2}{Z_1 + Z_2}\right)\int_0^X (X_{kR} - X_{kL})dx \end{array} \right] \end{array} \right\} = 0,$$

where u and v denote the two velocity components, in the x and y directions respectively. Obviously, $v_1 = v_2 = 0$ in the configuration of Figure 1.

Let us consider phase 1 equation (k = 1). The volume fraction equation becomes,

$$\frac{\partial \alpha_1}{\partial t} + \frac{1}{V}\left\{ \begin{array}{l} \left(\frac{Z_1 u_1 + Z_2 u_2}{Z_2 + Z_1} + \frac{p_2 - p_1}{Z_1 + Z_2}\right) \sum_{\text{vertical segments}} \int_{y_{\text{begin segment}}}^{y_{\text{end segment}}} (1-0)dy \\ + N_{\text{number of fluid channels}} \left[\left(\frac{p_1 - p_2}{Z_1 + Z_2}\right)\int_0^X (0-1)dx - \left(\frac{p_1 - p_2}{Z_1 + Z_2}\right)\int_0^X (1-0)dx \right] \end{array} \right\} = 0$$

Expanding the integrals,

$$\frac{\partial \alpha_1}{\partial t} + \frac{1}{XY}\left\{ \begin{array}{l} \left(\frac{Z_1 u_1 + Z_2 u_2}{Z_2 + Z_1} + \frac{p_2 - p_1}{Z_1 + Z_2}\right)(\alpha_{1R} - \alpha_{1L})Y \\ N_{\text{number of fluid channels}} \left[-\left(\frac{p_1 - p_2}{Z_1 + Z_2}\right)X - \left(\frac{p_1 - p_2}{Z_1 + Z_2}\right)X \right] \end{array} \right\} = 0$$

Therefore,

$$\frac{\partial \alpha_1}{\partial t}+\left(\frac{Z_1u_1+Z_2u_2}{Z_2+Z_1}+\frac{p_2-p_1}{Z_1+Z_2}\right)\frac{(\alpha_{1R}-\alpha_{1L})}{X}=\left(\frac{p_1-p_2}{Z_1+Z_2}\right)\frac{2N_{\text{number of fluid channel}}X}{XY}$$

In the limit when X tends to zero and denoting that the ratio $\frac{2N_{\text{number of fluid channel}}X}{XY}$ represents the specific interfacial area, the following result is obtained:

$$\frac{\partial \alpha_1}{\partial t}+\left(\frac{Z_1u_1+Z_2u_2}{Z_2+Z_1}+\frac{p_2-p_1}{Z_1+Z_2}\right)\frac{\partial \alpha_1}{\partial x}=\frac{A_I}{Z_1+Z_2}(p_1-p_2) \qquad \text{(III.3)}$$

This calculation method was already used in Saurel et al. (2003) where the various details may be found for the full set of equations. Equation (III.3) assumes positive volume fraction gradient ($\frac{\partial \alpha_1}{\partial x}\geq 0$). Generalized form is given in the same reference.

It is thus appears that the topological equation (III.3) used in BN is valid only in specific situations of stratified flows, annular ones, interfacial flows (Saurel and Abgrall, 1999), and possibly in packed granular beds where both phases are in contact and able to propagate sound.

In the present work we precisely examine alternative options.

Let us consider liquid drops suspended in a gas phase. The radius R_1 of a single spherical compressible liquid drop surrounded by a gas evolves with the following transport equation:

$$\frac{d_1R_1}{dt}=\mu_0(p_1-p_2) \qquad \text{(III.4)}$$

where μ_0 control the rate at which pressures equilibrate.

Indeed, the liquid being compressible, the spherical drop changes radius in accordance with the external pressure. Equation (III.4) implies,

$$\frac{\partial V_1}{\partial t}+u_1\frac{\partial V_1}{\partial x}=4\mu_0R_1^2(p_1-p_2), \qquad \text{(III.5)}$$

where $V_1=\frac{4}{3}\pi R_1^3$ denotes the volume of the drop.

In the absence of fragmentation and coalescence, the specific number of drops per unit volume obeys the following balance equation:

$$\frac{\partial N_1}{\partial t}+\frac{\partial N_1u_1}{\partial x}=0, \qquad \text{(III.6)}$$

where N_1 represents the specific number of drops.

Multiplying (III.5) by N_1 yields,

$$\frac{\partial \alpha_1}{\partial t}+\frac{\partial \alpha_1u_1}{\partial x}=\frac{3\alpha_1}{R_1}\mu_0(p_1-p_2) \qquad \text{(III.7)}$$

as $\alpha_1=N_1V_1$.

It is interesting to consider the symmetric situation of liquid containing spherical bubbles.

In this situation the bubble radius evolves according to,

$$\frac{d_2R_2}{dt}=\mu_{0'}(p_2-p_1),$$

and the specific number of bubbles per unit volume obeys the balance law,

$$\frac{\partial N_2}{\partial t}+\frac{\partial N_2u_2}{\partial x}=0.$$

Consequently the volume fraction equation reads,

$$\frac{\partial \alpha_2}{\partial t} + \frac{\partial \alpha_2 u_2}{\partial x} = \frac{3\alpha_2}{R_2} \mu_{0'} (p_2 - p_1) \qquad \text{(III.8)}$$

We now examine the implications of such volume fraction equations (III.7 and III.8) on the flow model.

IV. The new model

The new model is built in order to fulfill mass balance equations of each phase as well as conservation of the mixture momentum and mixture energy. It is also asked that the model agree with the second law of thermodynamics and causality principle through hyperbolicity condition.
The starting point of the derivation thus consists in the following set of partial differential equations.

a) Starting point of the derivation

For the moment dissipation is removed. Volume fraction equation (III.7) is considered (in the absence of pressure relaxation) in conjunction with basic balance equations:

$$\begin{aligned}
&\frac{\partial \alpha_1}{\partial t} + \frac{\partial \alpha_1 u_1}{\partial x} = 0, \\
&\frac{\partial (\alpha\rho)_1}{\partial t} + \frac{\partial (\alpha\rho u)_1}{\partial x} = 0, \\
&\frac{\partial (\alpha\rho)_2}{\partial t} + \frac{\partial (\alpha\rho u)_2}{\partial x} = 0, \qquad \text{(IV.1)} \\
&\frac{d_1 s_1}{dt} = 0, \\
&\frac{d_2 s_2}{dt} = 0, \\
&\frac{\partial (\alpha_1\rho_1 u_1 + \alpha_2\rho_2 u_2)}{\partial t} + \frac{\partial (\alpha_1\rho_1 u_1^2 + \alpha_1 p_1) + (\alpha_2\rho_2 u_2^2 + \alpha_2 p_2)}{\partial x} = 0, \\
&\frac{\partial (\alpha_1\rho_1 E_1 + \alpha_2\rho_2 E_2)}{\partial t} + \frac{\partial \alpha_1 u_1 (\rho_1 E_1 + p_1) + \alpha_2 u_2 (\rho_2 E_2 + p_2)}{\partial x} = 0.
\end{aligned}$$

From System (IV.1) the aim is now to determine evolution equations for the motion of each phase and associated energy balance equations.

b) Derivation

The momentum equations are assumed to be of the form,

$$\alpha_k \rho_k \frac{d_k u_k}{dt} + \frac{\partial \alpha_k p_k}{\partial x} = p_I \frac{\partial \alpha_k}{\partial x},$$

where p_I has to be determined.

The corresponding kinetic energy equations read:

$$\alpha_k \rho_k \frac{d_k \frac{u_k^2}{2}}{dt} + u_k \frac{\partial \alpha_k p_k}{\partial x} = p_I u_k \frac{\partial \alpha_k}{\partial x}.$$

In System (IV.1) the entropy equations read,

$$\frac{d_k s_k}{dt} = 0$$

i.e,

$$\frac{d_k e_k}{dt} - \frac{p_k}{\rho_k{}^2}\frac{d_k \rho_k}{dt} = 0.$$

The mass equations can also be written as,

$$\frac{d_k \rho_k}{dt} = -\frac{\rho_k}{\alpha_k}\frac{d_k \alpha_k}{dt} - \rho_k \frac{\partial u_k}{\partial x}.$$

Consequently,

$$\alpha_k \rho_k \frac{d_k e_k}{dt} + \frac{\partial \alpha_k p_k u_k}{\partial x} - \alpha_k u_k \frac{\partial p_k}{\partial x} + p_k \frac{\partial \alpha_k}{\partial t} = 0.$$

Summing the kinetic and internal energy equations of a given phase the corresponding total energy equation is obtained:

$$\frac{\partial \alpha_k \rho_k E_k}{\partial t} + \frac{\partial \alpha_k \rho_k u_k E_k}{\partial x} + \frac{\partial \alpha_k p_k u_k}{\partial x} + p_k \frac{\partial \alpha_k}{\partial t} = (p_I - p_k) u_k \frac{\partial \alpha_k}{\partial x}$$

Summing now the two phases total energy equations the mixture energy equation is obtained:

$$\frac{\partial \alpha_1 \rho_1 E_1 + \alpha_2 \rho_2 E_2}{\partial t} + \frac{\partial \alpha_1 \rho_1 u_1 E_1 + \alpha_2 \rho_2 u_2 E_2}{\partial x} + \frac{\partial \alpha_1 p_1 u_1 + \alpha_2 p_2 u_2}{\partial x}$$

$$+(p_1 - p_2)\frac{\partial \alpha_1}{\partial t} = p_I (u_1 - u_2)\frac{\partial \alpha_1}{\partial x} - p_1 u_1 \frac{\partial \alpha_1}{\partial x} + p_2 u_2 \frac{\partial \alpha_1}{\partial x}$$

Mixture energy conservation requires,

$$(p_1 - p_2)\frac{\partial \alpha_1}{\partial t} = \left[(p_I - p_1)u_1 - (p_I - p_2)u_2\right]\frac{\partial \alpha_1}{\partial x} \qquad \text{(IV.2)}$$

A sufficient condition appears, independently of the volume fraction equation:

$$p_I = p_1 = p_2 \qquad \text{(IV.3)}$$

This condition has to be understood at leading order, in the limit of stiff pressure relaxation. To be more precise let us consider first order expansions for the pressures:

$$p_k = p_k^0 + \varepsilon p_k^1 + ... \qquad \text{(IV.4)}$$

where ε is of the order of the inverse of the pressure relaxation coefficient μ. Therefore

$$\varepsilon \approx \frac{1}{\mu} \to 0^+.$$

The compatibility condition (IV.2) reads,

$$\left(p_1^0 - p_2^0 + \varepsilon\left(p_1^1 - p_2^1\right)\right)\frac{\partial \alpha_1}{\partial t} = \left[\left(p_I^0 - p_1^0 + \varepsilon\left(p_I^1 - p_1^1\right)\right)u_1 - \left(p_I^0 - p_2^0 + \varepsilon\left(p_I^1 - p_2^1\right)\right)u_2\right]\frac{\partial \alpha_1}{\partial x}$$

It is satisfied provided that,

$$p_I^0 = p_1^0 = p_2^0$$

It doesn't mean that pressure fluctuations disappear in the flow model. For example, volume fraction equation (III.8) becomes in this limit,

$$\frac{\partial \alpha_1}{\partial t} + \frac{\partial \alpha_1 u_1}{\partial x} = \frac{3\alpha_1}{R_1}\mu_0\left((p_1^0 - p_2^0) + \varepsilon(p_1^1 - p_2^1)\right) = p_1^1 - p_2^1,$$

Indeed, pressure relaxation parameter is present in this equation and tends to infinity:

$$\mu = \frac{3\alpha_1}{R_1}\mu_0 = \frac{1}{\varepsilon} \to +\infty.$$

It is also worth to mention, that, thanks to the volume fraction equation of System (IV.1), the mass and energy balance equations of the same phase reduce to (in the absence of relaxation effects),

$$\frac{d_1\rho_1}{dt} = 0 \qquad \text{(IV.3)}$$

and,

$$\frac{d_1 e_1}{dt} = 0\,. \qquad \text{(IV.4)}$$

c) Model summary

From the previous analysis the following flow model is obtained. Mechanical relaxation terms and heat transfer have been inserted for the sake of generality.

$$\begin{aligned}
&\frac{\partial \alpha_1}{\partial t} + \frac{\partial \alpha_1 u_1}{\partial x} = \mu(p_1 - p_2)\,,\\
&\frac{\partial (\alpha\rho)_1}{\partial t} + \frac{\partial (\alpha\rho u)_1}{\partial x} = 0\,,\\
&\frac{\partial \alpha_1\rho_1 u_1}{\partial t} + \frac{\partial \alpha_1\rho_1 u_1^2 + \alpha_1 p_1}{\partial x} = p_2\frac{\partial \alpha_1}{\partial x} + \lambda(u_2 - u_1)\,,\\
&\frac{\partial \alpha_1\rho_1 e_1}{\partial t} + \frac{\partial \alpha_1\rho_1 u_1 e_1}{\partial x} = -\mu p_2(p_1 - p_2) + \lambda\frac{Z_2}{Z_1 + Z_2}(u_2 - u_1)^2 + H(T_2 - T_1)\,,\\
&\frac{\partial (\alpha\rho)_2}{\partial t} + \frac{\partial (\alpha\rho u)_2}{\partial x} = 0\,,\\
&\frac{\partial (\alpha_1\rho_1 u_1 + \alpha_2\rho_2 u_2)}{\partial t} + \frac{\partial (\alpha_1\rho_1 u_1^2 + \alpha_1 p_1) + (\alpha_2\rho_2 u_2^2 + \alpha_2 p_2)}{\partial x} = 0\,,\\
&\frac{\partial (\alpha_1\rho_1 E_1 + \alpha_2\rho_2 E_2)}{\partial t} + \frac{\partial \alpha_1 u_1(\rho_1 E_1 + p_1) + \alpha_2 u_2(\rho_2 E_2 + p_2)}{\partial x} = 0\,.
\end{aligned} \qquad \text{(IV.5)}$$

The two relaxation parameters λ and μ are the same as in the BN model of Section II. 'H' represents the heat exchange coefficient, given by a correlation based on the Nusselt number and multiplied by the exchange interfacial area. Justification of dissipation effects modelling is given in Appendix A.

The associated mixture entropy equation reads,

$$\frac{\partial \alpha_1\rho_1 s_1 + \alpha_2\rho_2 s_2}{\partial t} + \frac{\partial \alpha_1\rho_1 s_1 u_1 + \alpha_2\rho_2 s_2 u_2}{\partial x} = \mu(p_1 - p_2)^2\left(\frac{1}{T_1} + \frac{1}{T_2}\right) + \lambda\frac{(u_2 - u_1)^2}{Z_1 + Z_2}\left(\frac{Z_2}{T_1} + \frac{Z_1}{T_2}\right) + \frac{H(T_2 - T_1)^2}{T_1 T_2} \qquad \text{(IV.6)}$$

Consequently the mixture entropy has non-negative production and the model is thermodynamically consistent, provided that pressure relaxation is stiff. Stiff pressure relaxation is valid for most applications (see Kapila et al., 2001 for relaxation times estimates). Obviously, System (IV.5) can be complemented by mass transfer. For the moment it is important to check hyperbolicity of the equations.

d) Hyperbolicity

Let's write system (IV.5) under the form,

$$\frac{\partial W}{\partial t} + A(W)\frac{\partial W}{\partial x} = 0\,,$$

with,

$$W = (\rho_1,\ s_1,\ s_2,\ \alpha_1,\ u_1,\ \rho_2,\ u_2)^T\,.$$

The Jacobian matrix reads,

$$A(W)=\begin{pmatrix} u_1 & 0 & 0 & 0 & 0 & 0 & 0 \\ 0 & u_1 & 0 & 0 & 0 & 0 & 0 \\ 0 & 0 & u_2 & 0 & 0 & 0 & 0 \\ 0 & 0 & 0 & u_1 & \alpha_1 & 0 & 0 \\ \dfrac{c_1^2}{\rho_1} & \dfrac{1}{\rho_1}\dfrac{\partial p_1}{\partial s_1}\Big)_{\rho_1} & 0 & 0 & u_1 & 0 & 0 \\ 0 & 0 & 0 & \dfrac{\rho_2}{\alpha_2}(u_1-u_2) & \dfrac{\alpha_1}{\alpha_2}\rho_2 & u_2 & \rho_2 \\ 0 & 0 & \dfrac{1}{\rho_2}\dfrac{\partial p_2}{\partial s_2}\Big)_{\rho_2} & 0 & 0 & \dfrac{c_2^2}{\rho_2} & u_2 \end{pmatrix}.$$

The wave speeds, solution of $|A-\lambda I|=0$ are,

$$\lambda_{1-4}=u_1,\ \lambda_5=u_2,\ \lambda_6=u_2-c_2 \text{ and } \lambda_7=u_2+c_2\ . \qquad \text{(IV.6)}$$

All roots being real the system is unconditionally hyperbolic. The wave speeds correspond to the one of the dilute model of Marble (1963) (Systems II.2 – II.3) and not those of Baer and Nunziato (1986), as expected.

e) Asymptotic limit

We now address stiff pressure and velocity relaxation limit to check compatibility of the model with the Kapila et al. (2001) one. This is important for the computation of material interfaces with capturing methods.

The pressure evolution equations read,

$$\frac{\partial p_1}{\partial t}+u_1\frac{\partial p_1}{\partial x}=-\frac{\rho_1 c_1^2}{\alpha_1}\mu(p_1-p_2)$$

$$\frac{\partial p_2}{\partial t}+u_2\frac{\partial p_2}{\partial x}+\frac{\rho_2 c_2^2}{\alpha_2}\frac{\partial \alpha_1 u_1+\alpha_2 u_2}{\partial x}=\frac{\rho_2 c_2^2}{\alpha_2}\mu(p_1-p_2)$$

Taking the difference,

$$u_1\frac{\partial p_1}{\partial x}-u_2\frac{\partial p_2}{\partial x}-\frac{\rho_2 c_2^2}{\alpha_2}\frac{\partial \alpha_1 u_1+\alpha_2 u_2}{\partial x}=-\left(\frac{\rho_1 c_1^2}{\alpha_1}+\frac{\rho_2 c_2^2}{\alpha_2}\right)\mu(p_1-p_2).$$

In the stiff pressure ($p_1^0=p_2^0=p^0$) and velocity relaxation limit ($u_1=u_2=u$),

$$\mu(p_1-p_2)\to\frac{\dfrac{\rho_2 c_2^2}{\alpha_2}}{\dfrac{\rho_1 c_1^2}{\alpha_1}+\dfrac{\rho_2 c_2^2}{\alpha_2}}\frac{\partial u}{\partial x}$$

Inserting this result in the volume fraction equation:

$$\frac{\partial \alpha_1}{\partial t}+u\frac{\partial \alpha_1}{\partial x}=\frac{\dfrac{\rho_1 c_1^2-\rho_2 c_2^2}{\alpha_2}}{\dfrac{\rho_1 c_1^2}{\alpha_1}+\dfrac{\rho_2 c_2^2}{\alpha_2}}\frac{\partial u}{\partial x}$$

The volume fraction equation of the Kapila et al. (2001) model is recovered.

It means that the present flow model is able to compute interfacial flows with the help of stiff velocity and pressure relaxation solvers. This feature is particularly important for the sake of generality of the formulation.

When stiff pressure relaxation is imposed strictly ($p_1 = p_2 = p$) and velocities maintained out of equilibrium, the well-known 6-equation model with two velocities and a single pressure is recovered. However, such a model is not hyperbolic (Guidaglia et al., 2001).

The present model is hyperbolic but not symmetric, as sound propagates only with the second phase. It is therefore interesting to compute relevant test problems to examine typical solutions. To do this, an appropriate computational solver is needed.

V. Hyperbolic solver

We address derivation of a Godunov type method for System (IV.5). In the absence of source terms, it can be written in compact form as,

$$\frac{\partial U}{\partial t}+\frac{\partial F(U)}{\partial x}+H(U)\frac{\partial \alpha_1}{\partial x} = 0 \qquad \text{(V.1)}$$

where,

$$U=\left(\alpha_1,\ \alpha_1\rho_1,\ \alpha_1\rho_1u_1,\ \alpha_1\rho_1e_1,\ \alpha_2\rho_2,\ (\alpha_1\rho_1u_1+\alpha_2\rho_2u_2),\ (\alpha_1\rho_1E_1+\alpha_2\rho_2E_2)\right)^T,$$

$$F(U)=\begin{pmatrix} \alpha_1u_1 \\ \alpha_1\rho_1u_1 \\ \alpha_1\rho_1u_1^2+\alpha_1p \\ \alpha_1\rho_1u_1e_1 \\ \alpha_2\rho_2u_2 \\ (\alpha_1\rho_1u_1{}^2+\alpha_2\rho_2u_2{}^2)+p \\ (\alpha_1\rho_1u_1E_1+\alpha_2\rho_2u_2E_2)+(\alpha_1u_1+\alpha_2u_2)p \end{pmatrix} \text{ and } H(U)=\begin{pmatrix} 0 \\ 0 \\ -p \\ 0 \\ 0 \\ 0 \\ 0 \end{pmatrix}$$

The difficulty with this hyperbolic system relies in the non-conservative terms $H(U)\frac{\partial \alpha_1}{\partial x}$.

For the sake of simplicity the Rusanov (1962) approximate Riemann solver is considered. It uses the following estimate for the right facing wave, at a given cell boundary separating cells i and i+1:

$$S = \mathrm{Max}_k\left(|\lambda_k|_{i+1}, |\lambda_k|_i\right)$$

At a given cell boundary separating left (L) and right (R) states, the flux solution reads,

$$F^* = \frac{1}{2}\left[F_R + F_L - S\left(U_R - U_L\right)\right] \qquad \text{(V.2)}$$

The Godunov scheme for System (V.1) necessarily reads,

$$U_i^{n+1} = U_i^n - \frac{\Delta t}{\Delta x}\left(F^*_{i+1/2} - F^*_{i-1/2}\right) + \Delta t A \qquad \text{(V.3)}$$

where A is the numerical approximation of $H(U)\frac{\partial \alpha_1}{\partial x}$, to be determined.

To determine an admissible approximation of A, we follow Saurel and Abgrall (1999) where a flow in uniform mechanical equilibrium is considered:

$$u_{1,i-1} = u_{1,i} = u_{1,i+1} = u_{2,i-1} = u_{2,i} = u_{2,i+1} = u > 0$$

$$p_{1,i-1} = p_{1,i} = p_{1,i+1} = p_{2,i-1} = p_{2,i} = p_{2,i+1} = p$$

Inserting the Rusanov flux (V.2) in the Godunov method (V.3) for the mass equation of the first phase, the following result is obtained:

$$(\alpha_1\rho_1)_i^{n+1} = (\alpha_1\rho_1)_i^n - \frac{u\Delta t}{2\Delta x}\left[(\alpha_1\rho_1)_{i+1} - (\alpha_1\rho_1)_{i-1}\right] + \frac{S\Delta t}{2\Delta x}\left[(\alpha_1\rho_1)_{i+1} - 2(\alpha_1\rho_1)_i + (\alpha_1\rho_1)_i\right] \tag{V.4}$$

The same procedure is done for the momentum equation of the same phase:

$$(\alpha_1\rho_1 u_1)_i^{n+1} = u\overbrace{\left[(\alpha_1\rho_1)_i^n - \frac{u\Delta t}{2\Delta x}\left[(\alpha_1\rho_1)_{i+1} - (\alpha_1\rho_1)_{i-1}\right] + \frac{S\Delta t}{2\Delta x}\left[(\alpha_1\rho_1)_{i+1} - 2(\alpha_1\rho_1)_i + (\alpha_1\rho_1)_i\right]\right]}^{(\alpha_1\rho_1)_i^{n+1}}$$

$$-\frac{\Delta t}{2\Delta x}p\left[\alpha_{1,i+1} - \alpha_{1,i-1}\right] + A$$

In order that $u_{1,i}^{n+1} = u$, the non-conservative term A must be approximated as,

$$A = p\frac{\alpha^*_{1,i+1/2} - \alpha^*_{1,i-1/2}}{\Delta x} \text{ with } \alpha^*_{1,i+\frac{1}{2}} = \frac{\alpha_{1,i+1} + \alpha_{1,i}}{2}. \tag{V.5}$$

The numerical scheme thus consists in (V.3) with (V.2) and (V.5), and is consequently very simple.

VI. Computed results

The first test corresponds to the simple transport of a volume fraction discontinuity in a flow field in uniform pressure and velocity equilibrium. The former method is extended to higher order thanks to the MUSCL algorithm (see for example Toro, 1997). Present computations use Minmod limiter.

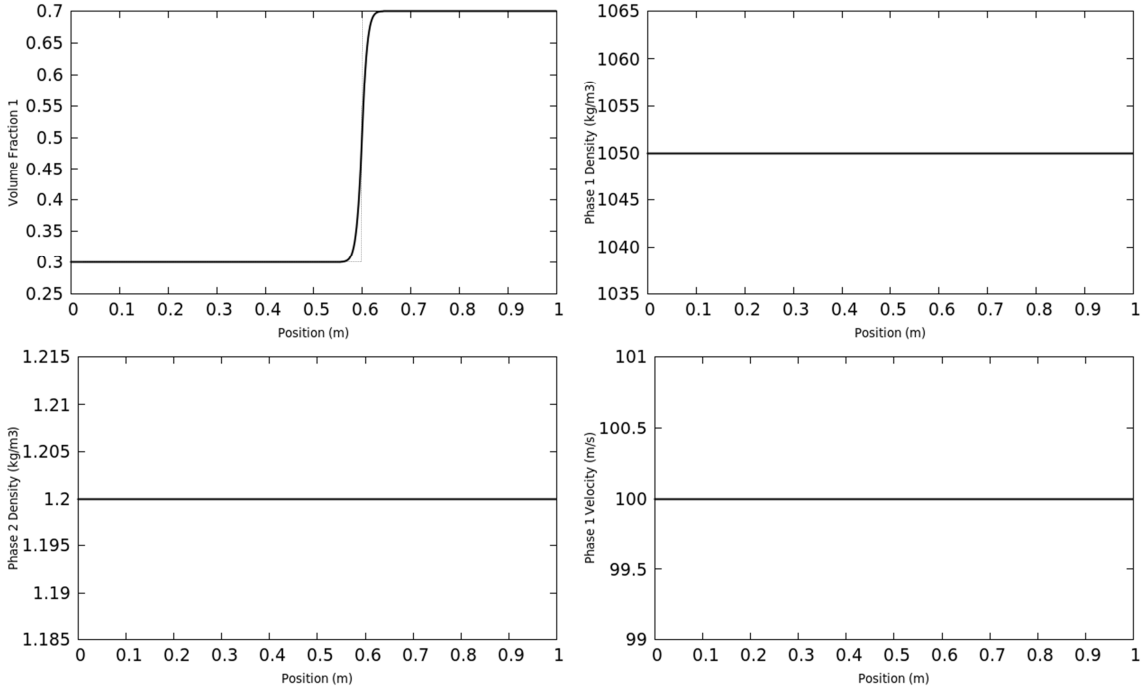

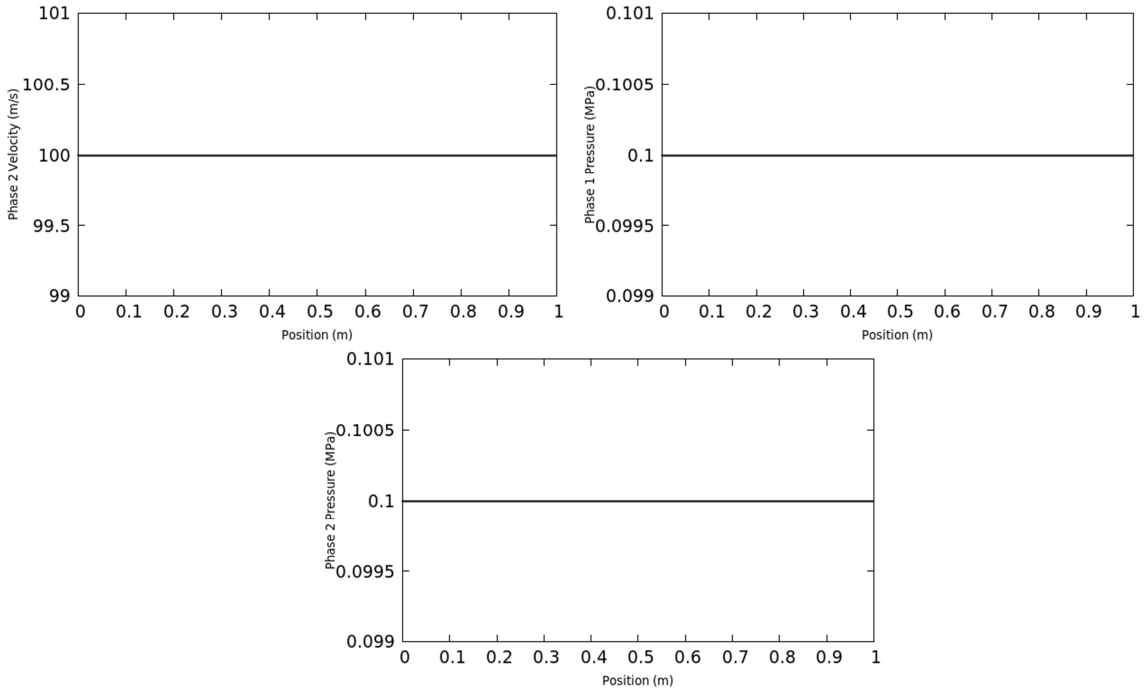

Figure 2. Volume fraction transport in uniform pressure and velocity fields. The mesh involves 500 cells and the time step is computed with CFL=0.5. Initial velocities are set to 100m/s and pressures are constant and equal to 10^5 Pa. The volume fraction discontinuity is initially set at 0.5 m. The numerical solution is plotted at 1ms. The exact solution for the volume fraction is presented in dot symbols showing perfect agreement. The numerical solutions are free of velocity and pressure spurious oscillations.

Another test is now addressed and corresponds to a two phase shock tube, as shown in Figure 3.

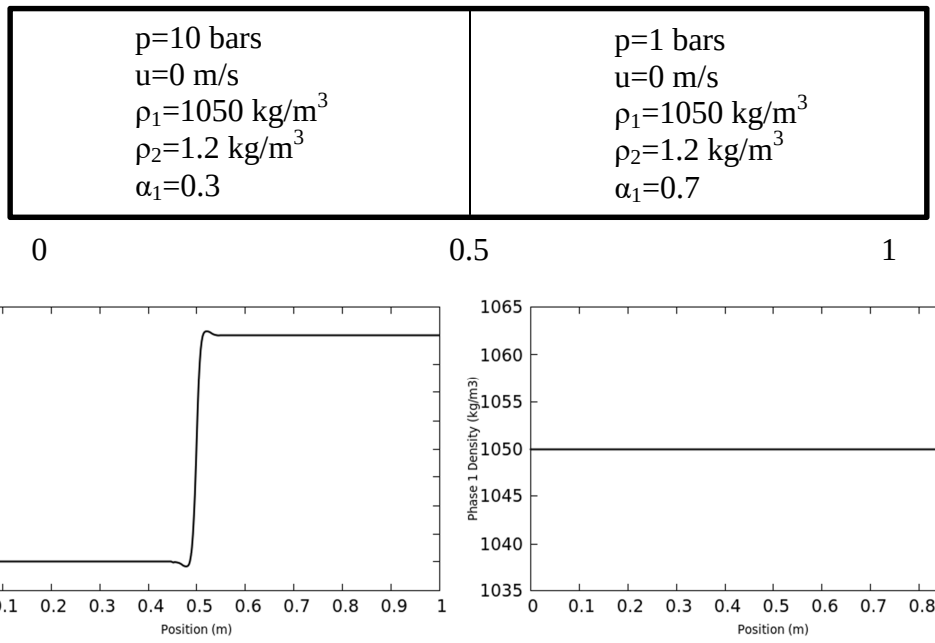

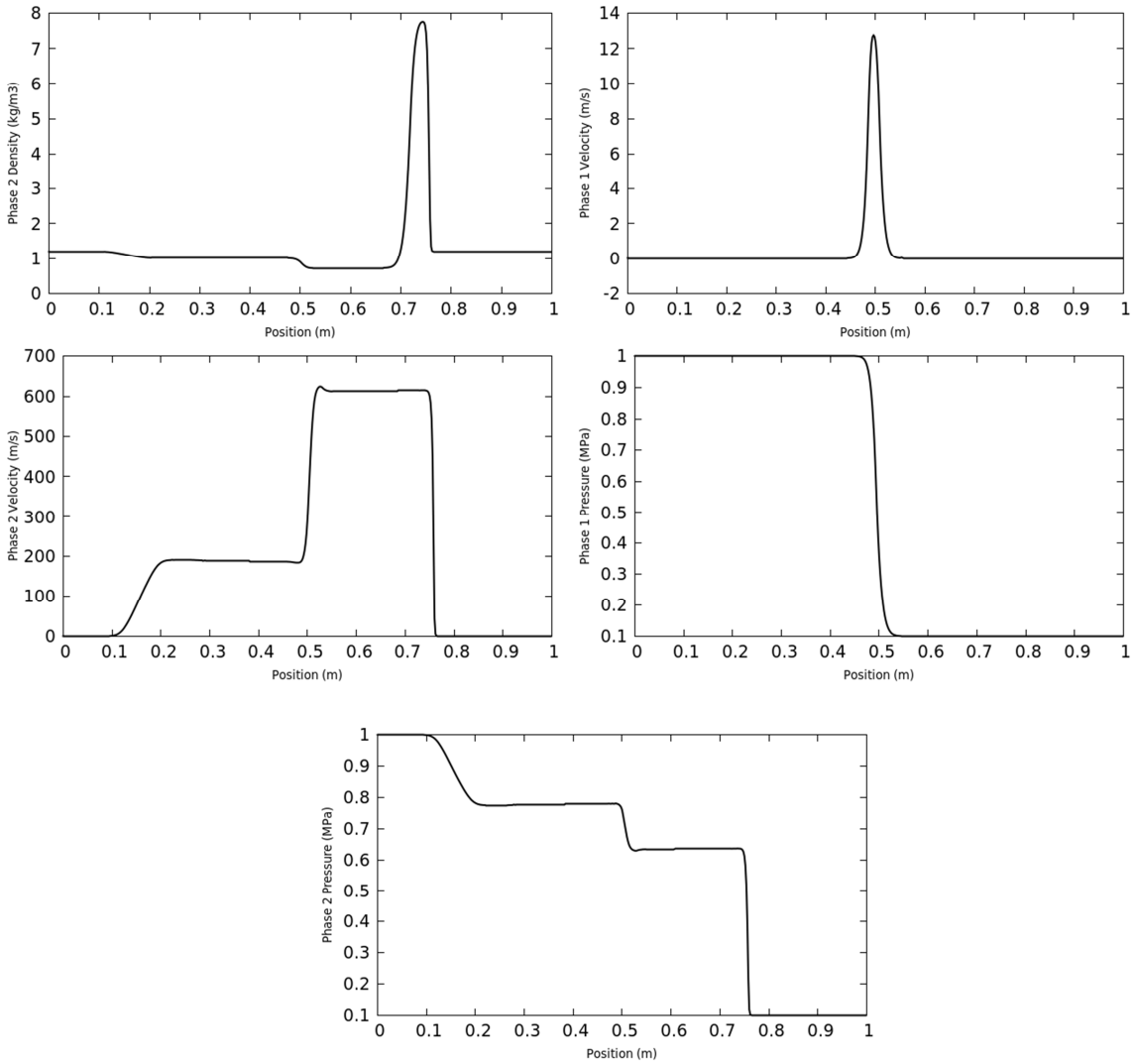

Figure 3. Smooth shock tube computations in the absence of relaxation terms. Computations are made with 500 cells and CFL=0.5. Computed results are shown at time 350μs. Four waves are visible, in spite of the simplified Riemann solver that considers two only. It is interesting to note the discontinuous profile of pressure in the phase 1: no pressure wave is present in this phase. Also note phase 1 velocity creation even in absence of drag effects. The pressure term in the momentum equation is responsible for that behavior.

These typical profiles are very different to those expected with BN and Marble models. For example, the pressure profiles of the phases are very different and even unphysical. The pressure of phase 1 must relax with the one of phase 2. Stiff pressure relaxation is thus mandatory. Pressure and velocity relaxation solvers are recalled in Appendix B.
The same run as the one defined in Figure 3 is reconsidered hereafter with pressure relaxation. The results are shown in Figure 4.

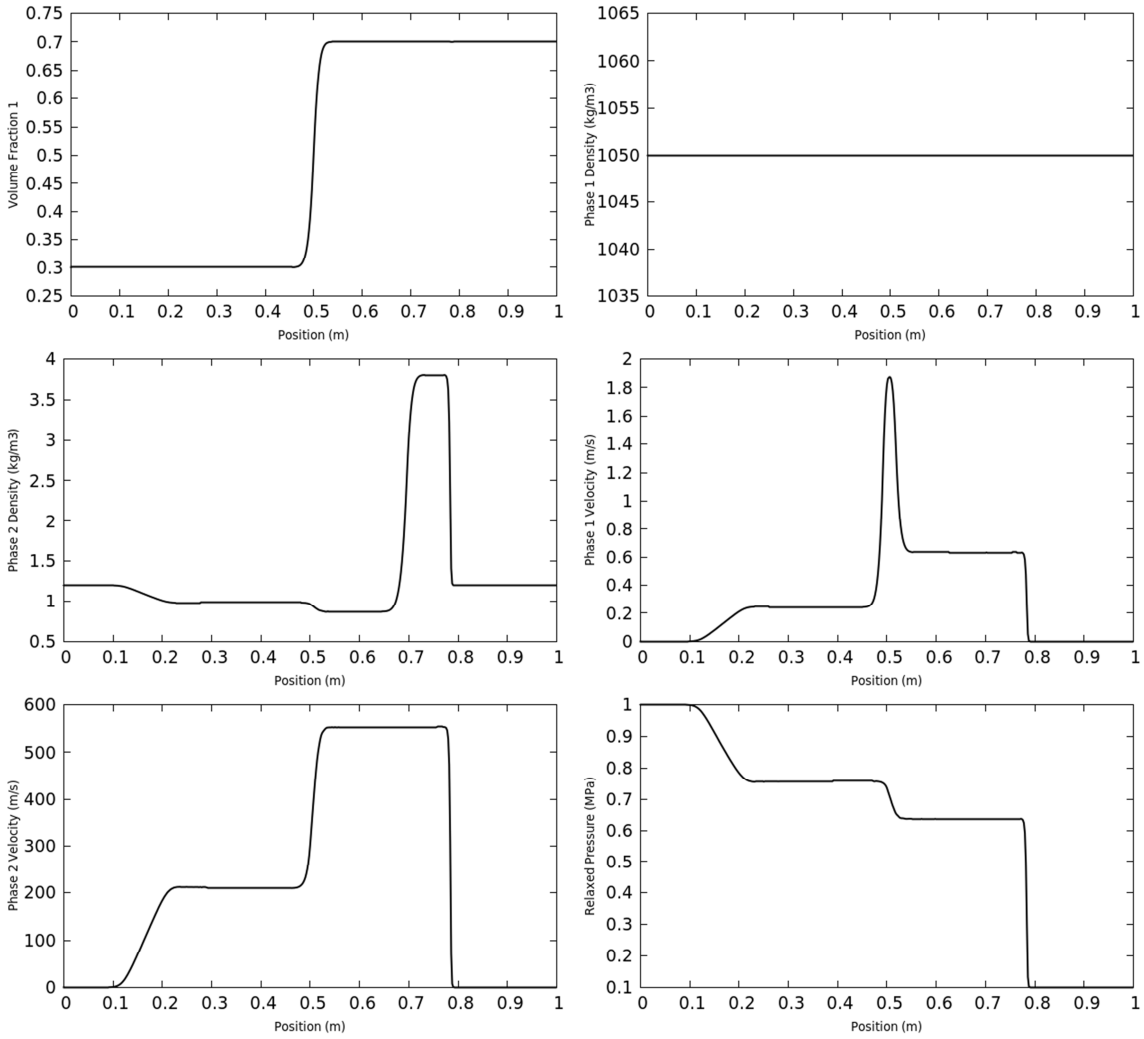

Figure 4. Smooth shock tube computations in the absence of velocity relaxation but with stiff pressure relaxation. Computations made with 500 cells and CFL=0.5. Computed results are shown at time 350μs. All pressures are now equal, modifying significantly the phase 1 velocity profile.

With the help of both velocity and pressure relaxation solvers it is possible to address interfaces separating (nearly) pure liquid and (nearly) pure gas. The aim is to analyze the behavior of the flow model in such limit case, having in mind it has been derived more to deal with clouds of drops than interfaces. The initial conditions are given in Figure 5 and correspond to a liquid at right set to motion by a pressurized gas at left. The exact solution is available for this test case and used to check predictions accuracy.

p=10 000 bars u=0 m/s ρ_1=1050 kg/m^3 ρ_2=100 kg/m^3 α_1=0.0001	p=1 bars u=0 m/s ρ_1=1050 kg/m^3 ρ_2=100 kg/m^3 α_1=0.9999

0 0.6 1

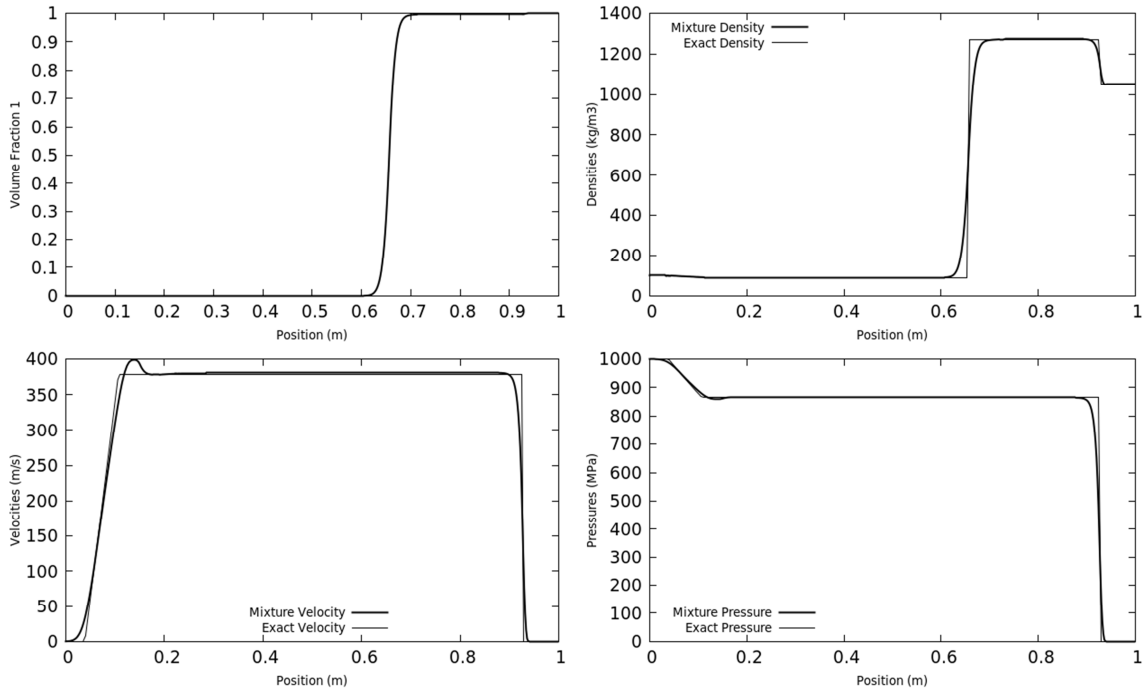

Figure 5. Shock tube with gas-liquid interface: High pressure gas at left and low pressure liquid at right. Computations done with 500 cells and CFL=0.5. Computed results shown at time 150μs. Both velocities and pressure are relaxed, making the interface condition of equal pressures and velocities fulfilled.

The same test is considered but with fluids in reverse order: High pressure liquid at left and low pressure gas at right. Corresponding results are shown in Figure 6 and compared to the exact solution.

p=10 000 bars u=0 m/s ρ_1=1050 kg/m^3 ρ_2=100 kg/m^3 α_1=0.9999	p=1 bars u=0 m/s ρ_1=1050 kg/m^3 ρ_2=100 kg/m^3 α_1=0.0001

0 0.7 1

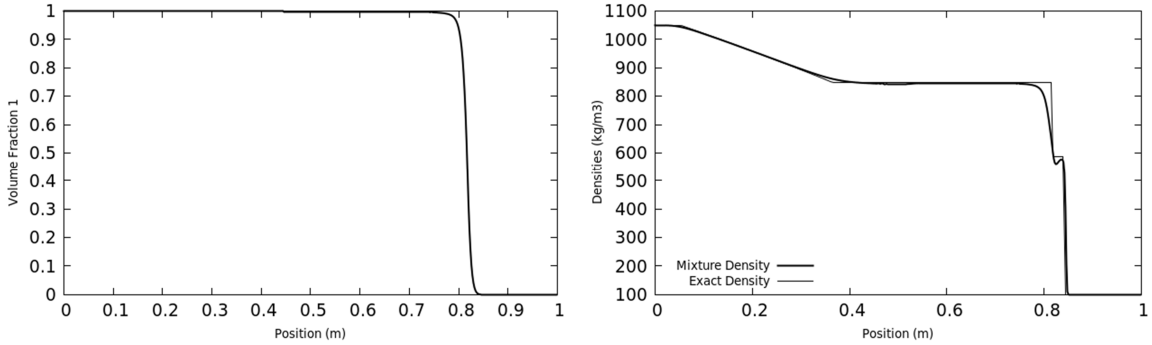

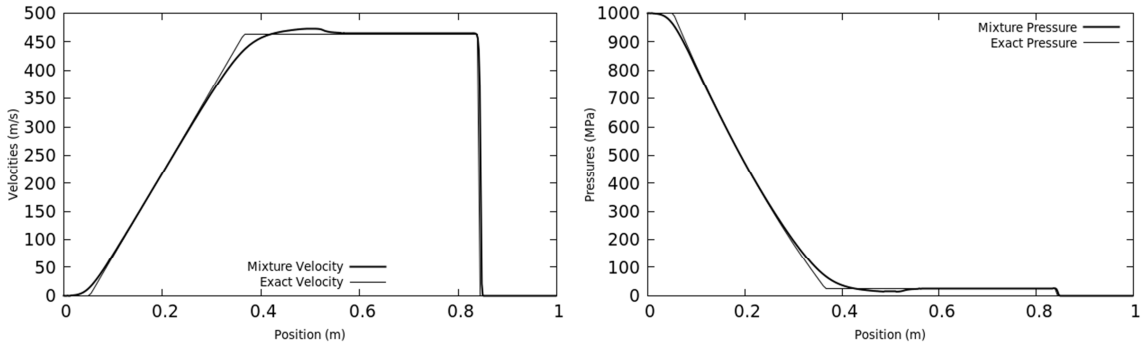

Figure 6. Shock tube with liquid-gas interface: high pressure liquid at left and low pressure gas at right. Computations done with 500 cells and CFL=0.5. Computed results shown at time 250μs. Both velocities and pressure are relaxed, making the interface condition of equal pressures and velocities fulfilled. However, convergence difficulties appear.

Convergence difficulties appear with this last test case. This is not surprising as physically a strong expansion wave propagates in the liquid while the flow model considers only sound propagation in the gas phase. Another reason for this poor agreement is due to the volume fraction equation, devised to consider droplet clouds and not interfaces.
Such test shows that the model and method are robust even when used out of their range of validity and design.
Therefore we now consider a test more appropriate to the model. It consists in the fluidization of a particle cloud under shock wave interaction. Such a configuration has been studied experimentally by Rogue et al. (1998) and is summarized in Figure 7.

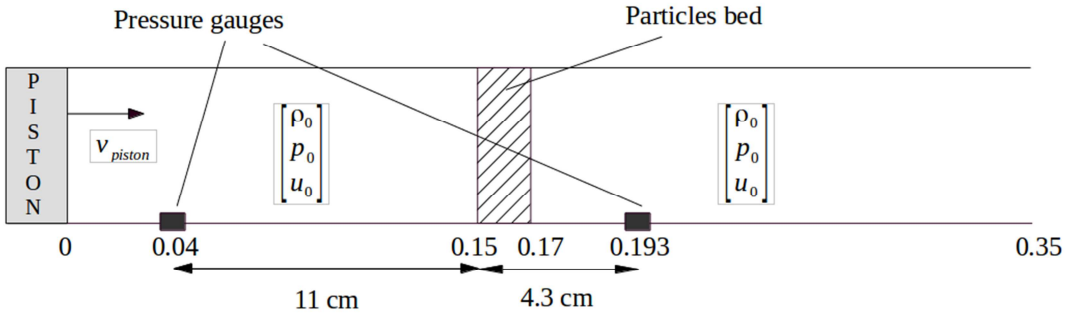

Figure 7. Rogue et al. (1998) fluidization shock tube test. A shock tube is filled with gas at density 1.2 kg/m^3. A dense cloud of glass particles ($\rho_0 = 1050 \text{kg/m}^3$) is set in a cross section of the tube, with 2 cm width. The initial solid volume fraction in the particle bed is 0.65. The initial pressure is uniform initially and set at 10^5 Pa. A shock at Mach number 1.3 is created by the expansion of the high pressure gas, corresponding to a shock created by a piston moving at 151 m/s. Treating the left boundary as a piston condition enables computational savings.

In this experiment pressure is recorded before and after the particles cloud, to examine reflected and transmitted waves through the granular media as well as its dilution and dispersion.
To account for drag effects, the following correlation is used in the phase 1 momentum equation:

$$F = \frac{6\alpha_1}{d_1} C_d \left(u_1 - u_2\right)$$

with,

$$C_d = 1 + 0.15 R_e^{0.687} \text{ and } R_e = \frac{\rho_2 \left|u_2 - u_1\right| d_1}{\mu_2}$$

The particle diameter appearing in these relation is constant ($d_1 = 1.5mm$) and the gas viscosity is $\mu_2 = 18\,10^{-6}$ Pa.s.

Thanks to this update, the predictions of the BN, Marble and new model are compared. The BN model, or more precisely its symmetric version with 7 waves is solved with the Furfaro and Saurel (2015) method. The Marble model is solved with the Saurel et al. (1994) method and the new model is solved with the method presented above.

Let us first comment Rogue et al. (1998) experimental data, typical pressure signals being shown in Figure 8.

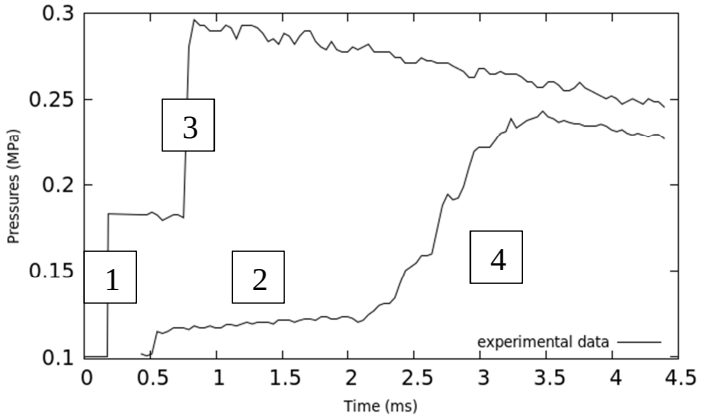

Figure 8. Experimental pressures signals of Rogue (1998): 1 denotes the incident shock wave, 2 denotes the transmitted shock wave, 3 denotes the reflected shock wave, 4 corresponds to the arrival of the cloud upper front at the pressure gauge location.

Computed results with the various models are shown in Figure 9.

(Marble)

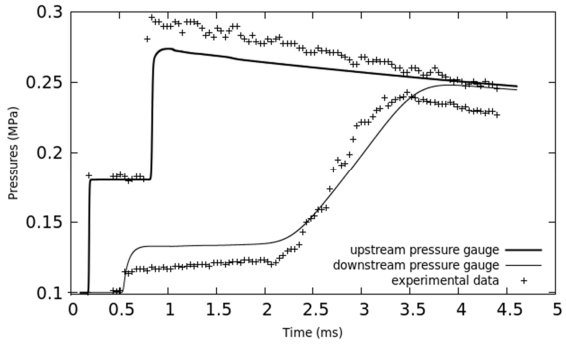

(BN)

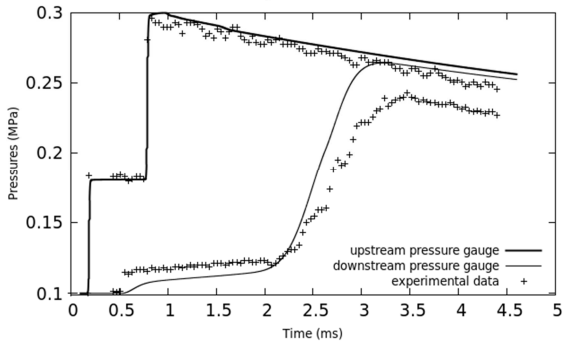

(Present)

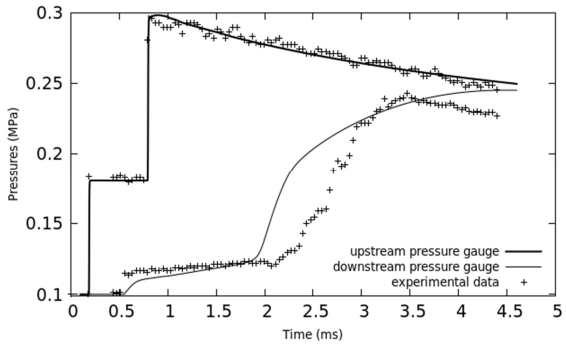

Figure 9. Comparison of computed results with the various model versus experimental data for the Rogue test problem. Computations are done with 500 cells and CFL=0.5. The van Leer flux limiter is used. Reflected and transmitted waves are badly predicted by the Marble model, but pressure evolution during particle cloud motion seems quite accurate. Wave transmission and reflection is better with BN but particle cloud dynamics loses accuracy. The best wave transmission and reflection is obtained with the new model, but cloud's dynamics is the worst.

Under mesh refinement, no modification of the conclusions appeared. At this stage, some potential appeared with the new model, but weakness emerged when considering liquid gas interfaces in severe conditions and for particle cloud dynamics in the Rogue test.
A symmetric variant of the new model, with Equation (III.8) instead of (III.7) is thus developed and examined.

VII. Symmetric variant

In the new model examined and tested formerly pressure waves propagate with the gas sound speed. This behavior seems incorrect if the flow is mainly made of liquid with small gas bubbles. We thus address the symmetric variant of the previous model on the basis of the volume fraction equation (III.8). Following the same derivation method as previously the following flow model is obtained (dissipation is omitted for the sake of simplicity):

$$
\begin{aligned}
&\frac{\partial \alpha_2}{\partial t} + \frac{\partial \alpha_2 u_2}{\partial x} = 0, \\
&\frac{\partial (\alpha\rho)_2}{\partial t} + \frac{\partial (\alpha\rho u)_2}{\partial x} = 0 \\
&\frac{\partial \alpha_2\rho_2 u_2}{\partial t} + \frac{\partial \alpha_2\rho_2 u_2^2 + \alpha_2 p}{\partial x} = p\frac{\partial \alpha_2}{\partial x} \\
&\frac{\partial \alpha_2\rho_2 e_2}{\partial t} + \frac{\partial \alpha_2\rho_2 u_2 e_2}{\partial x} = 0 \\
&\frac{\partial (\alpha\rho)_1}{\partial t} + \frac{\partial (\alpha\rho u)_1}{\partial x} = 0, \\
&\frac{\partial (\alpha_1\rho_1 u_1 + \alpha_2\rho_2 u_2)}{\partial t} + \frac{\partial (\alpha_1\rho_1 u_1^2 + \alpha_2\rho_2 u_2^2 + p)}{\partial x} = 0, \\
&\frac{\partial (\alpha_1\rho_1 E_1 + \alpha_2\rho_2 E_2)}{\partial t} + \frac{\partial \left[(\alpha_1\rho_1 u_1 E_1 + \alpha_2\rho_2 u_2 E_2) + (\alpha_1 u_1 + \alpha_2 u_2) p \right]}{\partial x} = 0
\end{aligned}
\qquad \text{(VII.1)}
$$

Obviously this system implies,

$$\frac{d_1 s_1}{dt} = 0,$$

$$\frac{d_2 s_2}{dt} = 0,$$

and consequently is in agreement with the second law of thermodynamics.
This system is hyperbolic with wave's speeds:

$\lambda_{1-4} = u_2$, $\lambda_5 = u_1$, $\lambda_6 = u_1 - c_1$ and $\lambda_7 = u_1 + c_1$.

Let us examine its typical solutions on some test problems, as done previously.
The same shock tube test case as the one of Figure 6 is considered with liquid at left and gas at right. Computed results are compared against the exact solution at the same time 250μs.

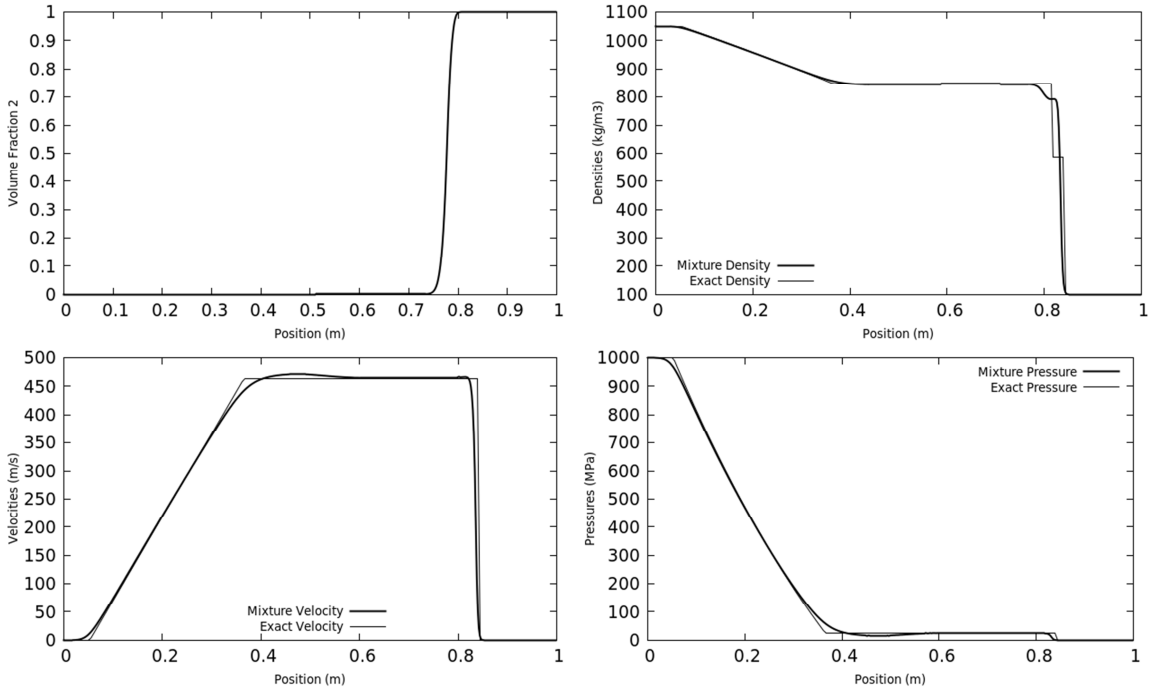

Figure 10. Liquid – gas shock tube test problem solved with the symmetric variant model with stiff pressure and velocity relaxation. Computations are done with 500 cells and CFL=0.5. Results are shown at time 250μs. The numerical solution tends to the exact one but converges difficultly.

It is interesting to compare the new model (System IV.5) and its symmetric variant (System VII.1) on a same computational test. This is done in Figure 11 where a two-phase shock tube with two different liquid-gas mixtures is considered.

p=1 000 bars u=0 m/s ρ_1=1050 kg/m^3 ρ_2=100 kg/m^3 α_1=0.2	p=1 bars u=0 m/s ρ_1=1050 kg/m^3 ρ_2=100 kg/m^3 α_1=0.8

0 0.5 1

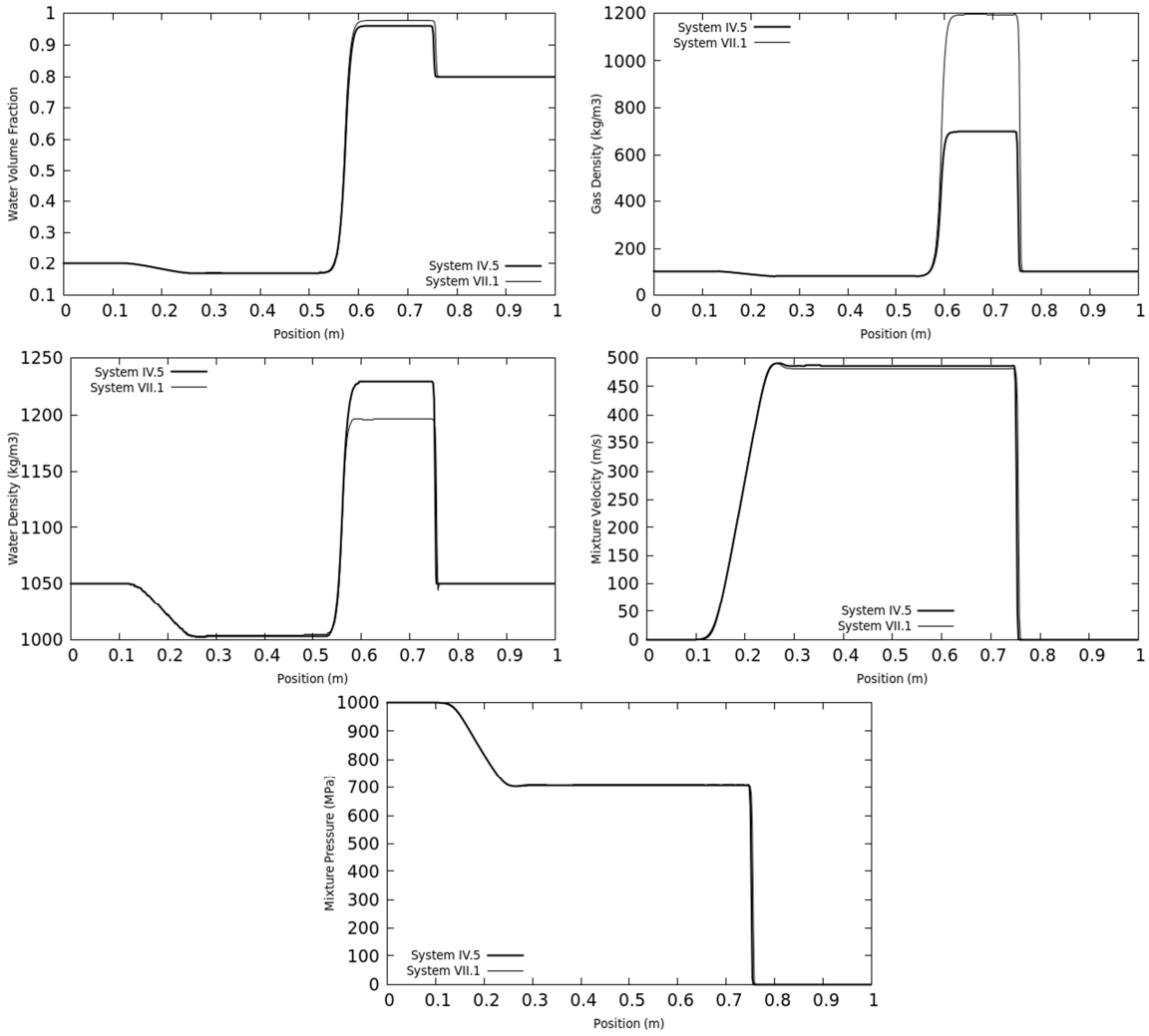

Figure 11. Comparison of the new model (IV.5) and its symmetric variant (VII.1) on the same two-phase shock tube test problem. Stiff velocity and pressure are used in both computations. As expected, differences are present.

It is also interesting to address the Rogue test problem with the symmetric variant model. Corresponding results are shown in Figure 12.

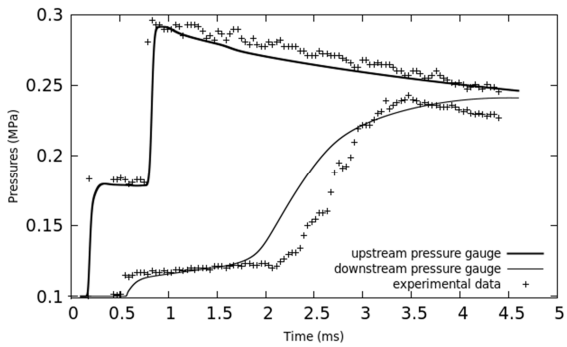

Figure 12. Computation of the Rogue test with the symmetric variant model and comparison with experimental pressure records. Computations are done with 500 cells and CFL=0.5. The van Leer flux limiter is used. Some accuracy has been lost in the incident and reflected waves compared to the original model while an interesting feature appears regarding the pressure rise during particle cloud motion that seems more accurate.

The lack of accuracy in the incident shock that propagates in a single phase gas media is certainly due to the absence of gas sound speed in the eigenvalues. The present formulation is derived for bubbly flows while it is used for a nearly pure gas in the first part of the shock tube.
As a summary of the various computational experiments, the symmetric variant model doesn't appear more accurate than the original version at least on the few test case considered herein. However,

- an interesting feature appeared with the Rogue test in relation with particle cloud motion,
- the presence of the phase 1 sound speed in the wave's speeds of this flow model is necessarily important when this phase is in dominant proportions.

Therefore an attempt for a general formulation is done in the section that follows.

VIII. Towards a general formulation

To embed the new model and its symmetric variant in a general formulation the following formulation is considered. Parameters 'a' and 'b' are defined as,

$$a = \begin{cases} 1 & \text{if} \quad \alpha_1 < \alpha^{\text{fluidization}} \\ 0 & \text{otherwize} \end{cases} \qquad \text{(VIII.1)}$$

$$b = a - 1$$

Parameter $\alpha^{\text{fluidization}}$ corresponds to some fluidization limit, for example $\alpha^{\text{fluidization}} \approx 0.5$.
Therefore, in this formulation 'a' and 'b' are local constants, but as they vary in the domain, $a = a(\alpha_1)$ and $b = b(\alpha_1)$.
The general flow model reads (in absence of dissipation),

$$\begin{aligned}
&\frac{\partial \alpha_1}{\partial t} + a\frac{\partial \alpha_1 u_1}{\partial x} + b\frac{\partial \alpha_2 u_2}{\partial x} = 0, \\
&\frac{\partial (\alpha\rho)_1}{\partial t} + \frac{\partial (\alpha\rho u)_1}{\partial x} = 0 \\
&\frac{\partial (\alpha\rho)_2}{\partial t} + \frac{\partial (\alpha\rho u)_2}{\partial x} = 0 \\
&\frac{\partial \alpha_1\rho_1 u_1}{\partial t} + \frac{\partial \alpha_1\rho_1 u_1^2 + \alpha_1 p}{\partial x} = p\frac{\partial \alpha_1}{\partial x} \\
&\frac{\partial \alpha_2\rho_2 u_2}{\partial t} + \frac{\partial \alpha_2\rho_2 u_2^2 + \alpha_2 p}{\partial x} = p\frac{\partial \alpha_2}{\partial x} \\
&\frac{\partial \alpha_1\rho_1 E_1}{\partial t} + \frac{\partial \alpha_1\rho_1 u_1 E_1}{\partial x} + \frac{\partial \alpha_1 u_1 p}{\partial x} = p\left(a\frac{\partial \alpha_1 u_1}{\partial x} + b\frac{\partial \alpha_2 u_2}{\partial x} \right) \\
&\frac{\partial \alpha_2\rho_2 E_2}{\partial t} + \frac{\partial \alpha_2\rho_2 u_2 E_2}{\partial x} + \frac{\partial \alpha_2 u_2 p}{\partial x} = -p\left(a\frac{\partial \alpha_1 u_1}{\partial x} + b\frac{\partial \alpha_2 u_2}{\partial x} \right)
\end{aligned} \qquad \text{(VIII.2)}$$

Obviously this system implies,

$$\frac{d_1 s_1}{dt} = 0,$$

$$\frac{d_2 s_2}{dt} = 0,$$

and is consequently thermodynamically consistent.
Insertion of dissipative effects is considered in Appendix A.
System (IX.2) can also be written as,

$$\frac{\partial W}{\partial t} + A(W)\frac{\partial W}{\partial x} = 0,$$

with,

$$W = \left(s_1,\ \ s_2,\ \ \alpha_1,\ \ \rho_1,\ \ u_1,\ \ \rho_2,\ \ u_2\right)^T,$$

and,

$$A(W) = \begin{pmatrix} u_1 & 0 & 0 & 0 & 0 & 0 & 0 \\ 0 & u_2 & 0 & 0 & 0 & 0 & 0 \\ \frac{1}{\rho_1}\frac{\partial p}{\partial s_1}\Big)_{\rho_1} & 0 & u_1 & \frac{c_1^2}{\rho_1} & 0 & 0 & 0 \\ 0 & 0 & -b\rho_1 & u_1 & b\frac{\rho_1}{\alpha_1}\left(u_2-u_1\right) & 0 & -b\rho_1\frac{\alpha_2}{\alpha_1} \\ 0 & 0 & a\alpha_1 & 0 & (au_1-bu_2) & 0 & b\alpha_2 \\ 0 & 0 & a\rho_2\frac{\alpha_1}{\alpha_2} & 0 & a\frac{\rho_2}{\alpha_2}(u_1-u_2) & u_2 & a\rho_2 \\ 0 & \frac{1}{\rho_2}\frac{\partial p}{\partial s_2}\Big)_{\rho_2} & 0 & 0 & 0 & \frac{c_2^2}{\rho_2} & u_2 \end{pmatrix}$$

This matrix has a nice structure. Eigenvalues are given by $\det(A-\lambda I)=0$ and result in the following polynomial,

$$\left[(u_2-\lambda)^2(u_1-\lambda)^2\left((au_1-bu_2)-\lambda\right)+(u_2-\lambda)^2bc_1^2\left((a-b)u_2-\lambda\right)+(u_1-\lambda)^2ac_2^2\left(\lambda+(b-a)u_1\right)\right]=0$$

When a=1, b=0 it reduces to,

$$(u_1-\lambda)^3\left[(u_2-\lambda)^2-c_2^2\right]=0$$

with the wave speeds of the first model.

When a=0, b=-1 it reduces to,

$$\left(u_2-\lambda\right)^3\left[(u_1-\lambda)^2-c_1^2\right]=0$$

with the wave speeds of the symmetric model.

Therefore the flow model (VIII.2) has the following wave speeds:

$$\lambda_1=u_1,\ \lambda_2=u_1+c_1,\ \lambda_3=u_1-c_1,\lambda_4=u_2,\ \lambda_5=u_2+c_2 \text{ and } \lambda_6=u_2-c_2\ . \qquad \text{(VIII.3)}$$

However, these wave speeds are not present at any point of space. They appear when the volume fraction crosses the fluidization limit ($\alpha^{\text{fluidization}}$) somewhere in the domain. In nearly all computational examples considered previously, such instance happens.

Let us mention that other guesses have been considered for parameters 'a' and 'b'. For example $a=\frac{1}{2}$, $b=-\frac{1}{2}$ yields imaginary wave speeds. Same observation appeared with $a=\alpha_2$, $b=-\alpha_1$.

For numerical computations, System (VIII.2) is expressed as,

$$\frac{\partial\alpha_1}{\partial t}+\frac{\partial\left(a\alpha_1u_1+b\alpha_2u_2\right)}{\partial x}-\left(\alpha_1u_1+\alpha_2u_2\right)\frac{\partial a}{\partial x}=0,$$

$$\frac{\partial(\alpha\rho)_1}{\partial t}+\frac{\partial(\alpha\rho u)_1}{\partial x}=0$$

$$\frac{\partial(\alpha\rho)_2}{\partial t}+\frac{\partial(\alpha\rho u)_2}{\partial x}=0$$

$$\frac{\partial\alpha_1\rho_1u_1}{\partial t}+\frac{\partial\alpha_1\rho_1u_1^2+\alpha_1p}{\partial x}=p\frac{\partial\alpha_1}{\partial x} \qquad \text{(VIII.4)}$$

$$\frac{\partial(\alpha\rho e)_1}{\partial t} + \frac{\partial(\alpha\rho eu)_1}{\partial x} = 0$$

$$\frac{\partial(\alpha\rho e)_2}{\partial t} + \frac{\partial(\alpha\rho eu)_2}{\partial x} = 0$$

$$\frac{\partial(\alpha_1\rho_1 u_1 + \alpha_2\rho_2 u_2)}{\partial t} + \frac{\partial(\alpha_1\rho_1 u_1^2 + \alpha_2\rho_2 u_2^2 + p)}{\partial x} = 0$$

$$\frac{\partial(\alpha_1\rho_1 E_1 + \alpha_2\rho_2 E_2)}{\partial t} + \frac{\partial\left[(\alpha_1\rho_1 u_1 E_1 + \alpha_2\rho_2 u_2 E_2) + (\alpha_1 u_1 + \alpha_2 u_2)p\right]}{\partial x} = 0$$

Derivatives of the function $a(\alpha_1)$ appear as it is not a constant.

It is solved with the hyperbolic solver of Section VI based on the Rusanov flux. However, the wave speed estimate,

$$S = \mathrm{Max}_k\left(|\lambda_k|_{i+1}, |\lambda_k|_i\right),$$

now involves the six eigenvalues (VIII.3).

Also System (VIII.4) involves three energy equations, one of them being obviously redundant. Overdeterminacy is however useful with respect to some computational issues (Babii et al., 2007, Godunov, 2008, Saurel et al., 2009).

The mixture energy equation and the phase 1 internal energy equations are used when $a = 1, b = 0$. The phase 2 internal energy is then reset with the relaxed pressure at the end of the time step.

When $a = 0, b = -1$, the mixture energy equation and the phase 2 internal energy equations are used. The phase 1 internal energy is then reset with the relaxed pressure at the end of the time step.

The volume fraction equation in (VIII.4) being now non conservative, appropriate scheme is needed. Similar analysis as the one described in Section V is reused. Details are given in Appendix C.

Let us examine typical solutions of the general model on some test problems, as those considered previously. A shock tube test case with liquid at left and gas at right is considered, in the same conditions as the tests in Figures 6 and 10. Computed results are compared against exact solution.

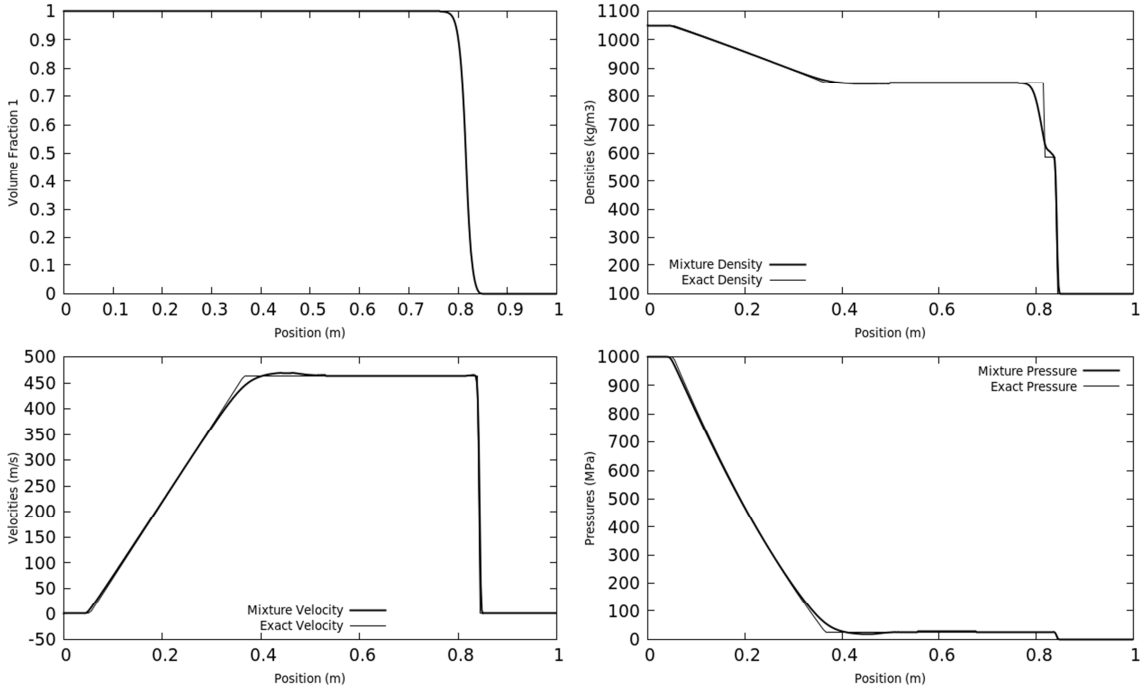

Figure 13. Liquid – gas shock tube test problem solved with the general model with stiff pressure and velocity relaxation. Computations are done with 500 cells and CFL=0.5. Results are shown at time 250μs. The numerical solution tends to the exact one and converges quite well. Compared to the original model results (Figure 6) and its symmetric variant results (Figure 10) improvements are visible especially for the velocities profile.

Let us now consider the reversed situation of gas-liquid shock tube already considered with the original model in Figure 5, where initial data are given. Comparison between computed results and exact solution is shown in Figure 14.

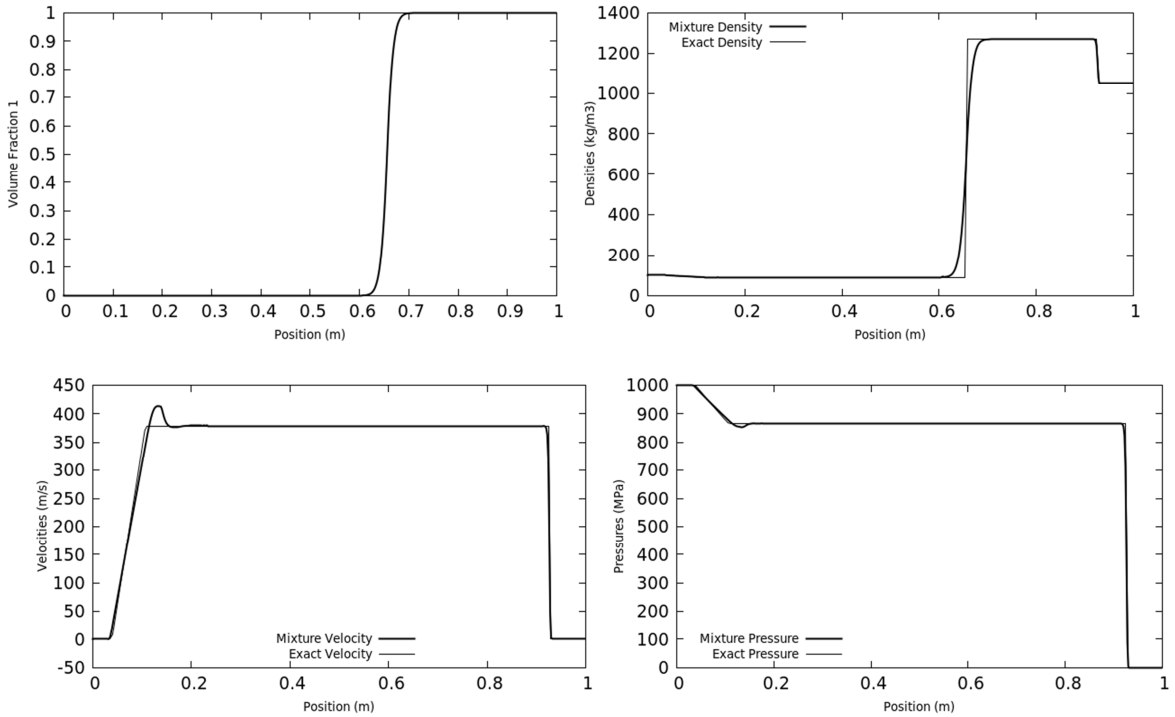

Figure 14. Shock tube with gas-liquid interface computed with the general model with stiff pressure and velocity relaxation. Computations done with 500 cells and CFL=0.5. Computed results are shown at time 150μs. Comparable accuracy as the one observed in Figure 5 with the original model is observed.

It is also interesting to address the Rogue test problem with the general model. Corresponding results are shown in Figure 15.

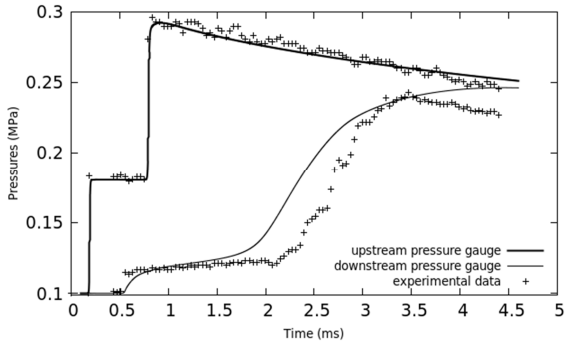

Figure 15. Computation of the Rogue test with the general model and comparison with experimental pressure records. Computations are done with 500 cells and CFL=0.5. The flux limiter used here is Minmod. The various transmitted and reflected waves are correctly computed and improvements appear regarding pressure evolution during particle cloud motion.

This last test shows improvements compared to Marble and BN models results:

- reflected and transmitted waves have better accuracy,
- pressure rise in the particle cloud shows comparable accuracy with respect to the existing models.

Intergranular stress (Bdzil et al., 1999, Saurel et al., 2010) has been considered as a possible effect to improve these computations. These effects have been added to the present formulation and coded, but no noticeable improvement appeared.

IX. Conclusion

A new two-phase hyperbolic and thermodynamically consistent model has been built and typical solutions have been computed.

It is able to compute the same flow configurations as the BN model, i.e. interfaces separating pure fluids and non-equilibrium multiphase mixtures. Its acoustic properties sound physical.

It is expected that two-phase shock waves structure be easier to analyze in the present frame. It is also expected that multidimensional solutions exhibit more differences than present one-dimensional computations, in particular regarding interface instabilities.

References

Ambroso, A., Chalons, C., & Raviart, P. A. (2012) A Godunov-type method for the seven-equation model of compressible two-phase flow. Computers & Fluids, 54, 67-91

Babii, D. P., Godunov, S. K., Zhukov, V. T., & Feodoritova, O. B. (2007). On the difference approximations of overdetermined hyperbolic equations of classical mathematical physics. Computational Mathematics and Mathematical Physics, 47(3), 427-441.

Baer, M. R., & Nunziato, J. W. (1986) A two-phase mixture theory for the deflagration-to-detonation transition (DDT) in reactive granular materials. International journal of multiphase flow, 12(6), 861-889

Bdzil, J. B., Menikoff, R., Son, S. F., Kapila, A. K., & Stewart, D. S. (1999). Two-phase modeling of deflagration-to-detonation transition in granular materials: A critical examination of modeling issues. Physics of Fluids 11(2), 378-402

Deledicque, V., & Papalexandris, M. V. (2007) An exact Riemann solver for compressible two-phase flow models containing non-conservative products. Journal of Computational Physics 222(1), 217-245

Furfaro, D., & Saurel, R. (2015) A simple HLLC-type Riemann solver for compressible non-equilibrium two-phase flows. Computers & Fluids, 111, 159-178

Ghidaglia, J. M., Kumbaro, A., & Le Coq, G. (2001) On the numerical solution to two fluid models via a cell centered finite volume method. European Journal of Mechanics-B/Fluids, 20(6), 841-867

Godunov, S. K. (2008). On approximations for overdetermined hyperbolic equations. In Hyperbolic Problems: Theory, Numerics, Applications (pp. 19-33). Springer Berlin

Houim, R. W., & Oran, E. S. (2016). A multiphase model for compressible granular–gaseous flows: formulation and initial tests. Journal of Fluid Mechanics, 789, 166-220

Kapila, A. K., Menikoff, R., Bdzil, J. B., Son, S. F., & Stewart, D. S. (2001) Two-phase modeling of deflagration-to-detonation transition in granular materials: Reduced equations. Physics of Fluids, 13(10), 3002-3024

Lhuillier, D., Chang, C. H., & Theofanous, T. G. (2013) On the quest for a hyperbolic effective-field model of disperse flows. Journal of Fluid Mechanics,731, 184-194

Marble, F.E (1963) Dynamics of a gas containing small solid particles. Combustion and Propulsion (5th AGARD Colloquium), Pergamon Press

McGrath II, T. P., Clair, J. G. S., & Balachandar, S. (2016). A compressible two-phase model for dispersed particle flows with application from dense to dilute regimes. Journal of Applied Physics, 119(17), 174903

Petitpas, F., Saurel, R., Franquet, E., & Chinnayya, A. (2009) Modelling detonation waves in condensed energetic materials: Multiphase CJ conditions and multidimensional computations. Shock waves, 19(5), 377-401

Rusanov, V. V. E. (1962). The calculation of the interaction of non-stationary shock waves and obstacles. USSR Computational Mathematics and Mathematical Physics 1(2), 304-320

Romenski, E., & Toro, E. F. (2004). Compressible two-phase flows: two-pressure models and numerical methods. Comput. Fluid Dyn. J, 13, 403-416

Saurel, R., Daniel, E., & Loraud, J. C. (1994) Two-phase flows-Second-order schemes and boundary conditions. AIAA Journal, 32(6), 1214-1221

Saurel, R., & Abgrall, R. (1999) A multiphase Godunov method for compressible multifluid and multiphase flows. Journal of Computational Physics, 150(2), 425-467

Saurel, R., Gavrilyuk, S., & Renaud, F. (2003). A multiphase model with internal degrees of freedom: Application to shock–bubble interaction. Journal Fluid Mech, 495, 283- 321

Saurel, R., Franquet, E., Daniel, E., & Le Metayer, O. (2007). A relaxation-projection method for compressible flows. Part I: The numerical equation of state for the Euler equations. Journal of Computational Physics, 223(2), 822-845

Saurel, R., Petitpas, F., & Berry, R. A. (2009). Simple and efficient relaxation methods for interfaces separating compressible fluids, cavitating flows and shocks in multiphase mixtures. Journal of Computational Physics, 228(5), 1678-1712

Saurel, R., Favrie, N., Petitpas, F., Lallemand, M. H., & Gavrilyuk, S. L. (2010) Modelling dynamic and irreversible powder compaction. Journal of Fluid Mechanics, 664, 348-396

Saurel, R., Le Martelot, S., Tosello, R., & Lapébie, E. (2014) Symmetric model of compressible granular mixtures with permeable interfaces. Physics of Fluids, 26(12), 123304

Schwendeman, D. W., Wahle, C. W., & Kapila, A. K. (2006) The Riemann problem and a high-resolution Godunov method for a model of compressible two-phase flow. Journal of Computational Physics, 212(2), 490-526

Zeldovich, Y.B. (1970) Gravitational instability: An approximate theory for large density perturbations. Astron. Astrophys, 5, 84–89

Appendix A. Inserting dissipation in the flow model

System (IV.5) contains dissipative effects and the aim of this appendix is to justify the modeling adopted. Also, insertion of same effects in the general model (VIII.2) is addressed.
Mass transfer is omitted, but velocity drag, pressure relaxation and heat exchanges are considered. For the sake of generality, System (VIII.2) is considered, formulations for System (IV.5) and its symmetric variant (VII.1) are deduced just setting (a=1, b=0) and (a=0, b=1) respectively.
The following system is speculated as dissipative extension of System (VIII.2):

$$
\begin{aligned}
&\frac{\partial \alpha_1}{\partial t} + a\frac{\partial \alpha_1 u_1}{\partial x} + b\frac{\partial \alpha_2 u_2}{\partial x} = \mu(p_1 - p_2),\\
&\frac{\partial (\alpha\rho)_1}{\partial t} + \frac{\partial (\alpha\rho u)_1}{\partial x} = 0\\
&\frac{\partial (\alpha\rho)_2}{\partial t} + \frac{\partial (\alpha\rho u)_2}{\partial x} = 0\\
&\frac{\partial \alpha_1\rho_1 u_1}{\partial t} + \frac{\partial \alpha_1\rho_1 u_1^2 + \alpha_1 p_1}{\partial x} = p_I\frac{\partial \alpha_1}{\partial x} + \lambda(u_2 - u_1)\\
&\frac{\partial \alpha_2\rho_2 u_2}{\partial t} + \frac{\partial \alpha_2\rho_2 u_2^2 + \alpha_2 p_2}{\partial x} = p_I\frac{\partial \alpha_2}{\partial x} - \lambda(u_2 - u_1)
\end{aligned}
\qquad (A.1)
$$

$$\frac{\partial \alpha_1\rho_1 E_1}{\partial t}+\frac{\partial \alpha_1\rho_1 u_1 E_1}{\partial x}+\frac{\partial \alpha_1 u_1 p_1}{\partial x}=p_{II}\left(a\frac{\partial \alpha_1 u_1}{\partial x}+b\frac{\partial \alpha_2 u_2}{\partial x}\right)-p_{II}\mu(p_1-p_2)+\lambda u_I(u_2-u_1)+H(T_2-T_1)$$

$$\frac{\partial \alpha_2\rho_2 E_2}{\partial t}+\frac{\partial \alpha_2\rho_2 u_2 E_2}{\partial x}+\frac{\partial \alpha_2 u_2 p_2}{\partial x}=-p_{II}\left(a\frac{\partial \alpha_1 u_1}{\partial x}+b\frac{\partial \alpha_2 u_2}{\partial x}\right)+p_{II}\mu(p_1-p_2)-\lambda u_I(u_2-u_1)-H(T_2-T_1)$$

where p_I , p_{II} and u_I have to be determined.

This formulation obviously agrees with the mixture mass, momentum and energy constraints:

$$\begin{aligned}
&\frac{\partial(\alpha\rho)_1+(\alpha\rho)_2}{\partial t}+\frac{\partial(\alpha\rho u)_1+(\alpha\rho u)_2}{\partial x}=0,\\
&\frac{\partial(\alpha_1\rho_1 u_1+\alpha_2\rho_2 u_2)}{\partial t}+\frac{\partial(\alpha_1\rho_1 u_1{}^2+\alpha_1 p_1)+(\alpha_2\rho_2 u_2{}^2+\alpha_2 p_2)}{\partial x}=0,\\
&\frac{\partial(\alpha_1\rho_1 E_1+\alpha_2\rho_2 E_2)}{\partial t}+\frac{\partial \alpha_1 u_1(\rho_1 E_1+p_1)+\alpha_2 u_2(\rho_2 E_2+p_2)}{\partial x}=0.
\end{aligned} \qquad \text{(A.2)}$$

To determine the above mentioned interfacial variables, let's examine to entropy production in each phase and in the system.

Combining mass, momentum and energy equations of phase 1 results in:

$$\alpha_1\rho_1 T_1\frac{d_1 s_1}{dt}=(p_1-p_{II})\frac{\partial \alpha_1}{\partial t}+(p_1-p_I)u_1\frac{\partial \alpha_1}{\partial x}+\lambda(u_I-u_1)(u_2-u_1)+H(T_2-T_1)$$

Inserting the volume fraction equation it becomes,

$$\alpha_1\rho_1 T_1\frac{d_1 s_1}{dt}=\mu(p_1-p_2)(p_1-p_{II})-(p_1-p_{II})\left(a\frac{\partial \alpha_1 u_1}{\partial x}+b\frac{\partial \alpha_2 u_2}{\partial x}\right)$$

$$+(p_1-p_I)u_1\frac{\partial \alpha_1}{\partial x}+\lambda(u_I-u_1)(u_2-u_1)+H(T_2-T_1)$$

In the stiff pressure relaxation limit (at leading order),

$$p_I=p_1=p_2=p_{II}=p, \qquad \text{(A.3)}$$

many terms vanish in the entropy equation:

$$\alpha_1\rho_1 T_1\frac{d_1 s_1}{dt}=\mu(p_1-p_2)^2+\lambda(u_I-u_1)(u_2-u_1)+H(T_2-T_1) \qquad \text{(A.4)}$$

For the second phase, similar result is obtained:

$$\alpha_2\rho_2 T_2\frac{d_2 s_2}{dt}=\mu(p_1-p_2)^2+\lambda(u_2-u_I)(u_2-u_1)-H(T_2-T_1) \qquad \text{(A.5)}$$

Following Saurel et al. (2003) the drag force exert power at the interfacial speed,

$$u_I=\frac{Z_1u_1+Z_2u_2}{Z_1+Z_2}. \qquad \text{(A.6)}$$

Combining (A.4) and (A.5) with their mass equations and summing results in the following mixture entropy equation:

$$\frac{\partial \alpha_1\rho_1 s_1+\alpha_2\rho_2 s_2}{\partial t}+\frac{\partial \alpha_1\rho_1 s_1 u_1+\alpha_2\rho_2 s_2 u_2}{\partial x}=\mu(p_1-p_2)^2\left(\frac{1}{T_1}+\frac{1}{T_2}\right)+\lambda\frac{(u_2-u_1)^2}{Z_1+Z_2}\left(\frac{Z_2}{T_1}+\frac{Z_1}{T_2}\right)+\frac{H(T_2-T_1)^2}{T_1T_2}$$

Therefore Systems (A.1) with closure relations (A.3) and (A.6) is appropriate.

Appendix B. Stiff pressure and velocity relaxation solvers

a) Stiff pressure relaxation

The system to solve during pressure relaxation is the following:

$$\begin{cases} \dfrac{\partial \alpha_1}{\partial t} = \mu\left(p_1 - p_2\right) \\ \dfrac{\partial \alpha_1 \rho_1}{\partial t} = 0 \\ \dfrac{\partial \alpha_1 \rho_1 u_1}{\partial t} = 0 \\ \dfrac{\partial \alpha_1 \rho_1 e_1}{\partial t} = -\mu p\left(p_1 - p_2\right) \\ \dfrac{\partial \alpha_2 \rho_2}{\partial t} = 0 \\ \dfrac{\partial \alpha_1 \rho_1 u_1 + \alpha_2 \rho_2 u_2}{\partial t} = 0 \\ \dfrac{\partial \alpha_1 \rho_1 E_1 + \alpha_2 \rho_2 E_2}{\partial t} = 0 \end{cases}$$

where p denotes the relaxed pressure.

Combining the internal energy equation of phase 1 with the corresponding volume fraction equation results in,

$$\frac{\partial e_1}{\partial t} = -p\frac{\partial v_1}{\partial t}$$

where v is the specific volume of the considered phase.

Considering the relaxed pressure as a constant it becomes (this assumption has been analyzed in Saurel et al., 2007),

$$e_1^* - e_1^0 = -p\left(v_1^* - v_1^0\right) \tag{B.1}$$

The stiffened gas equation of state (any other convex EOS can be considered as an option) is inserted,

$$e_k\left(p_k, v_k\right) = \frac{p_k + \gamma_k p_{k\infty}}{\gamma_k - 1} v_k$$

Consequently (B.1) becomes,

$$\frac{p^* + \gamma_1 p_{1\infty}}{\gamma_1 - 1} v_1^* - \frac{p_1^0 + \gamma_1 p_{1\infty}}{\gamma_1 - 1} v_1^0 = -p^*\left(v_1^* - v_1^0\right)$$

I.e.,

$$\alpha_1^* = \alpha_1^0 + \frac{\alpha_1^0}{\gamma_1}\left(\frac{p_1^0 + p_{1\infty}}{p^* + p_{1\infty}} - 1\right) \tag{B.2}$$

Same result is obtained for the second phase,

$$\alpha_2^* = \alpha_2^0 + \frac{\alpha_2^0}{\gamma_2}\left(\frac{p_2^0 + p_{2\infty}}{p^* + p_{2\infty}} - 1\right)$$

The saturation constraint $\sum_{k=1}^{N} \alpha_1^* = 1$ is then considered resulting in the following root for the equilibrium pressure:

$$p^* = \frac{1}{2}\left(A_1 + A_2 - p_{1\infty} - p_{2\infty}\right) + \sqrt{\frac{1}{4}\left(A_2 - A_1 + p_{1\infty} - p_{2\infty}\right)^2 + A_1 A_2} \tag{B.3}$$

where, $A_1 = \dfrac{\dfrac{\alpha_1^0}{\gamma_1}\left(p_1^0 + p_{1\infty}\right)}{\dfrac{\alpha_1^0}{\gamma_1} + \dfrac{\alpha_2^0}{\gamma_2}}$ and $A_2 = \dfrac{\dfrac{\alpha_2^0}{\gamma_2}\left(p_2^0 + p_{2\infty}\right)}{\dfrac{\alpha_1^0}{\gamma_1} + \dfrac{\alpha_2^0}{\gamma_2}}$.

Once the relaxed pressure is determined with (B.3) the volume fractions at equilibrium are determined with (B.2). The density of the phases are then deduced as,

$$\rho_1^* = \frac{\alpha_1^0 \rho_1^0}{\alpha_1^*} \text{ and } \rho_2^* = \frac{\alpha_2^0 \rho_2^0}{1 - \alpha_1^*}$$

Last, the phase 1 internal energy is reset as,

$$e_1^* = e_1\left(\rho_1^*, p^*\right)$$

The internal energy of the second phase is extracted from the mixture total energy.
The opposite is done when the symmetric variant of the flow model is used.

b) Stiff velocities relaxation

During stiff velocity relaxation, the subsystem to consider reads,

$$\frac{\partial \alpha_1 \rho_1}{\partial t} = 0$$

$$\frac{\partial \alpha_1 \rho_1 u_1}{\partial t} = \lambda(u_2 - u_1)$$

$$\frac{\partial \alpha_1 \rho_1 e_1}{\partial t} = \lambda(u_2 - u_1)(u_I - u_1)$$

$$\frac{\partial \alpha_2 \rho_2}{\partial t} = 0$$

$$\frac{\partial \alpha_1 \rho_1 u_1 + \alpha_2 \rho_2 u_2}{\partial t} = 0$$

$$\frac{\partial \alpha_1 \rho_1 E_1 + \alpha_2 \rho_2 E_2}{\partial t} = 0$$

where u_I is defined by (A.6).

As $\lambda \to +\infty$ both velocities relax to the equilibrium one given by the mixture momentum equation,

$$u^* = \frac{\alpha_1 \rho_1 u_1 + \alpha_2 \rho_2 u_2}{\alpha_1 \rho_1 + \alpha_2 \rho_2}$$

The velocities of phases 1 is then reset as:

$$\alpha_1 \rho_1 u_1 = \left(\alpha_1^0 \rho_1^0\right) u^*$$

And the internal energy of the same phase by,

$$e_1 = e_1^0 + \left(\frac{Z_2}{Z_1 + Z_2}(u_2 - u_1)\right)^0 (u^* - u_1^0)$$

Such velocity relaxation modifies both kinetic and internal energies. Pressure relaxation is thus needed after velocity relaxation.

Appendix C. Derivation of the volume fraction numerical scheme for System (VIII.4)

The volume fraction equation,

$$\frac{\partial \alpha_1}{\partial t} + \frac{\partial\left(a \alpha_1 u_1 + b \alpha_2 u_2\right)}{\partial x} - \left(\alpha_1 u_1 + \alpha_2 u_2\right)\frac{\partial a}{\partial x} = 0,$$

must have a discretization compatible with the mass equation of the same system,

$$\frac{\partial(\alpha\rho)_1}{\partial t} + \frac{\partial(\alpha\rho u)_1}{\partial x} = 0.$$

In uniform velocity flows conditions, using the Rusanov flux (V.2) in the Godunov method (V.3), the discrete mass equation reads,

$$(\alpha_1\rho_1)_i^{n+1} = (\alpha_1\rho_1)_i^n - \frac{u\Delta t}{2\Delta x}\left[(\alpha_1\rho_1)_{i+1} - (\alpha_1\rho_1)_{i-1}\right] + \frac{S\Delta t}{2\Delta x}\left[(\alpha_1\rho_1)_{i+1} - 2(\alpha_1\rho_1)_i + (\alpha_1\rho_1)_{i-1}\right] \quad (C.1)$$

The same is done for the volume fraction equation,

$$(\alpha_1)_i^{n+1} = (\alpha_1)_i^n - \frac{u\Delta t}{2\Delta x}\left[(a\alpha_1 + b\alpha_2)_{i+1} - (a\alpha_1 + b\alpha_2)_{i-1}\right] + \frac{S\Delta t}{2\Delta x}\left[(\alpha_1)_{i+1} - 2(\alpha_1)_i + (\alpha_1)_{i-1}\right] + u\Delta t\frac{\Delta a}{\Delta x} \quad (C.2)$$

where $\frac{\Delta a}{\Delta x}$ is the numerical approximation of $\frac{\partial a}{\partial x} = 0$, to be determined.

Rearranging (C.2) with $b = a - 1$ and $\alpha_2 = 1 - \alpha_1$ the discrete volume fraction equation becomes,

$$(\alpha_1)_i^{n+1} = (\alpha_1)_i^n - \frac{u\Delta t}{2\Delta x}\left[\alpha_{1i+1} - \alpha_{1i-1}\right] - \frac{u\Delta t}{2\Delta x}\left[a_{i+1} - a_{i-1}\right] + \frac{S\Delta t}{2\Delta x}\left[(\alpha_1)_{i+1} - 2(\alpha_1)_i + (\alpha_1)_{i-1}\right] + u\Delta t\frac{\Delta a}{\Delta x} \quad (C.3)$$

Let us now consider the particular case of uniform density field: $\rho_{1,i}^{\ n} = \rho_{1,i+1}^{\ n} = \rho_{1,i-1}^{\ n}$.

Both velocity and density being uniform, the density at the next time step must be invariant: $\rho_{1,i}^{\ n+1} = \rho_{1,i}^{\ n}$. In this context, the mass equation becomes,

$$(\alpha_1\rho_1)_i^{n+1} = \rho_1\left\{(\alpha_1)_i^n - \frac{u\Delta t}{2\Delta x}\left[(\alpha_1)_{i+1} - (\alpha_1)_{i-1}\right] + \frac{S\Delta t}{2\Delta x}\left[(\alpha_1)_{i+1} - 2(\alpha_1)_i + (\alpha_1)_{i-1}\right]\right\} \quad (C.4)$$

In order that (C.3) and (C.4) be compatible it is necessary that,

$$-\frac{u\Delta t}{2\Delta x}\left[a_{i+1} - a_{i-1}\right] + u\Delta t\frac{\Delta a}{\Delta x} = 0$$

Therefore,

$$\frac{\Delta a}{\Delta x} = \frac{a_{i+1} - a_{i-1}}{2\Delta x} \quad (C.5)$$

or,

$$\frac{\Delta a}{\Delta x} = \frac{a_{i+1/2}^* - a_{i-1/2}^*}{\Delta x},$$

with $a_{i+1/2}^* = \frac{a_{i+1}^n + a_i^n}{2}$.

Consequently the volume fraction scheme reads,

$$\alpha_{1,i}^{n+1} = \alpha_{1,i}^n - \frac{\Delta t}{\Delta x}\left(F_{\alpha i+1/2}^* - F_{\alpha i-1/2}^*\right) + \left(\alpha_1 u_1 + \alpha_2 u_2\right)_i^n \Delta t\frac{\Delta a}{\Delta x} \quad (C.6)$$

with ,

$$F_{\alpha i+1/2}^* = \frac{1}{2}\left[\left(a\alpha_1 u_1 + b\,\alpha_2 u_2\right)_{i+1}^n + \left(a\alpha_1 u_1 + b\,\alpha_2 u_2\right)_i^n - S\left(\alpha_{1,i+1}^{\ n} - \alpha_{1,i}^{\ n}\right)\right].$$